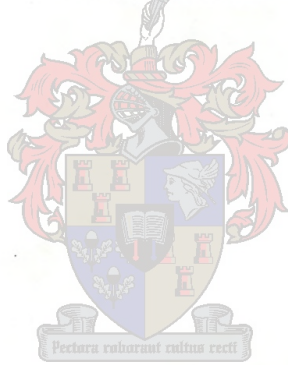# Higher Order Hierarchal Curvilinear Triangular Vector Elements for the Finite Element Method in Computational Electromagnetics

Neilen Marais

Thesis presented in partial fulfilment of the requirements for the degree of Master of Science in Engineering at the University of Stellenbosch.

Supervisor: Prof. D.B. Davidson

April 2003

Declaration

I, the under-signed, hereby declare that the work contained in this thesis is my own original work, unless indicated otherwise, and that it has not previously, in its entirety, or in part, been submitted at any university for a degree.

Neilen Marais

Date

Abstract

The Finite Element Method (FEM) as applied to Computational Electromagnetics (CEM), can be used to solve a large class of Electromagnetics problems with high accuracy, and good computational efficiency. Computational efficiency can be improved by using element basis functions of higher order. If, however, the chosen element type is not able to accurately discretise the computational domain, the converse might be true. This paper investigates the application of elements with curved sides, and higher order basis functions, to computational domains with curved boundaries. It is shown that these elements greatly improve the computational efficiency of the FEM applied to such domains, as compared to using elements with straight sides, and/or low order bases.

Opsomming

Die Eindige Element Metode (EEM) kan breedvoerig op Numeriese Elektromagnetika toegepas word, met uitstekende akkuraatheid en 'n hoë doeltreffendheids vlak. Numeriese doeltreffendheid kan verbeter word deur van hoër orde element basisfunksies gebruik te maak. Indien die element egter nie die numeriese domein effektief kan diskretiseer nie, mag die omgekeerde geld. Hierdie tesis ondersoek die toepassing van elemente met geboë sye, en hoër orde basisfunksies, op numeriese domeine met geboë grense. Daar word getoon dat sulke elemente 'n noemenswaardinge verbetering in die numeriese doeltreffendheid van die EEM meebring, vergeleke met reguit- en/of laer-orde elemente.

Acknowledgements

Contents

CONTENTS

CONTENTS

List of Tables

List of Figures

Chapter 1

Introduction

The Finite Element Method (FEM) is well established as an effective Computational Electromagnetics (CEM) method. The application of FEM to CEM is described in detail in texts such as [1], [2] and [3]. While the field is currently fairly well developed, developments which improve computational efficiency will always be sought.

In this paper, two relatively recent, such developments in the field are investigated, viz. using higher order vector element basis functions, and using curvilinear elements. While neither of these techniques are new to FEM in general, the latter is not widely described in the current electronic engineering literature.

1.1 Motivation for Higher Order Elements

It is well established that using vectorial, edge-based, curl conforming elements is currently the best approach for applying the FEM to most microwave problems [4], [1, §7.5], [2, §8]. These elements ameliorate the issues of spurious modal solutions, and poor modelling of singularities at metallic edges, commonly encountered when standard, node-based, scalar elements are extended to model vector valued EM field problems.

From conventional, scalar FEM experience, it is known that using basis functions of higher polynomial order, result in faster convergence with mesh size, and hence leads to better computational efficiency [5, §8]. Initially, the lowest-order vector elements, known as Whitney, or Constant Tangential Linear Normal (CT/LN) elements were most widely studied.

Defining higher order basis functions for vector elements are, however, somewhat more complex than for scalar elements. Initially, higher order basis functions were found in a somewhat ad hoc manner (ie. [6], [7].) More recently, systematic methods of defining interpolatory [8], and hierarchal [9], vector basis functions of arbitrary order have been published.

Higher order vector elements are very efficient. An element with a field

6

which has curl complete to polynomial order $(p-1)$, will show an energy error that is of order $O(h^{2p})$, where h is the element edge length used to discretise the problem [9].

With higher order elements being more efficient, simpler meshes may be used for a given level of accuracy. Since mesh generation, and processing, can be fairly time, and memory, consuming in its own right, this is a desirable property.

If a hierarchal basis is used, each element in a mesh need not have the same order of basis functions. Higher order elements may then be used only in the parts of a mesh where they yield the greatest benefit (p-adaption) [10] [11].

1.2 Motivation for Curvilinear Elements

In the previous section, it has been presupposed that the mesh used to discretise a computational domain, models the geometry of the problem exactly. Most published vector elements have straight sides. They are, therefore, incapable of modelling the geometry of any curved domain exactly.

High order bases stand to gain the most from using curved elements. With lower order elements, the improvement of the geometrical modelling error with h, is often commensurate with that of the field modelling.

The field modelling of higher order elements, on the other hand, is likely to converge much faster than the geometrical modelling provided by straight edges. Consequently, the rather rough geometrical modelling provided by straight elements dominates the solution accuracy [12], [13], [14].

Geometrical approximation error will also adversely affect p-adaption. P-adaption depends on the field being modelled more accurately over a given element, as the basis order is increased on that element. If the element lies on the edge of a curved domain, there is no escaping the geometrical error without refining the mesh.

1.3 Chapter Summary

Chapter 2 The basic FEM variational formulation is introduced, and the basics of implementing a vector FEM code is discussed.

Chapter 3 Curvilinear coordinates are introduced. It is shown how Covariant Projection Mapping may be used to construct curl-conforming vector elements.

Chapter 4 Discussion of the theory and implementation of higher order bases.

Chapter 5 Mappings that may be used with the theory of Chapter 3 are introduced.

Chapter 6 Description of parametric curves is given. They complement some of the methods described in Chapter 5.

Chapter 7 Results are presented, and analysed.

Chapter 8 The conclusion is presented.

Chapter 2

The Finite Element Method for Computational Electromagnetics: Theory and Implementation

This chapter presents an overview of the FEM, and the theory of its application to EM problems, given a variational formulation. Furthermore, the implementation of a basic 2-D vector-element FEM code, applicable to arbitrary shaped, homogeneous waveguides, is detailed. The rest of the work described in this document builds on the theory described in this chapter.

2.1 Finite Element Method Theory

The Finite Element Method (FEM) is a widely used and effective technique, for numerically obtaining approximate solutions to problems posed by the equations of calculus [5]. In particular, it is effective at the solution of partial-differential, boundary-value problems, such as those posed by many problems in electromagnetics.

2.1.1 A Brief History of the FEM

The basic principles on which the FEM is based, were first studied in the early 1940's. It was initially applied to mechanical problems such as heat conduction, mechanical stress/strain, and fluid-dynamics. As computers became cheaper, more powerful, and more plentiful, and sophisticated matrix techniques were developed, the FEM became very widely used.

In the mid-1960s, it was realised that the FEM was, in fact, a very broad numerical technique. Through the 1970's its mathematical basis was more rigorously established. This brought to light its applicability to any problem

9

that could be placed in variational form, or be defined by weighted residuals, or global energy balance principles.

Electromagetic field problems are defined in terms of partial differential equations, for which variational formulations are known. This led naturally to the FEM being applied to this field.

Straight forward application of previous FEM techniques (ie. nodal, scalar, elements) yielded some difficulties, most notably spurious, non-physical, mode solutions. These were overcome in the mid 1980's to early 1990's, with the introduction of vector elements [4], [15], [16], [17].

2.1.2 Variational Formulation of the Vector Helmholtz Equation for 2D Lossless Homogeneous Waveguide Field Problems

The starting point of a vector CEM FEM code is usually the vector wave equation, here in terms of the electric field, $\vec{E}$,

$$\nabla \times (\frac{1}{\mu} \nabla \times \vec{E}) - \omega^2 \epsilon_c \vec{E} = -j\omega \vec{J}_i, \qquad (2.1)$$

where μ and ϵ_c are, respectively, the permeability, and the complex permittivity, of the medium, $\vec{J}_i$ the impressed current, and ω the frequency in radians per second. $\epsilon_c = \epsilon - j\sigma/\omega$ includes the result of, both the induced conduction current ($\sigma \vec{E}$), with σ the conductivity of the medium, and the displacement current.

In the case of a source-free, lossless, inhomogeneous waveguide, with boundary conditions

$$\hat{n} \times \vec{E} = 0 \quad \text{on } \Gamma_1 \qquad (2.2)$$

$$\hat{n} \times (\nabla \times \vec{E}) = 0 \quad \text{on } \Gamma_2, \qquad (2.3)$$

where Γ_1 and Γ_2 refer, respectively, to electric and magnetic walls, we get

$$\nabla \times \left(\frac{1}{\mu_r} \nabla \times \vec{E} \right) - k_o^2 \epsilon_r \vec{E} = 0 \quad \text{in } \Omega, \qquad (2.4)$$

where μ_r and ϵ_r refer to, respectively, the relative permeability, and permittivity, of the medium, and the free space wave number, $k_0 = \omega\sqrt{(\epsilon_0 \mu_0)}$, has been substituted.

The equivalent variational problem, given real ϵ_r and μ_r, is solved by satisfying [2, §8.2]

$$\hat{n} \times \vec{E} = 0 \quad \text{on } \Gamma_1, \qquad (2.5)$$

and rendering stationary the functional

$$F(\vec{E}) = \frac{1}{2} \iint\limits_{\Omega} \left[\frac{1}{\mu_r} (\nabla \times \vec{E}) \cdot (\nabla \times \vec{E})^* - k_0^2 \epsilon_r \vec{E} \cdot \vec{E}^* \right] d\Omega. \qquad (2.6)$$

10

Assuming a known z-dependence as $\vec{E}(x,y,z) = \vec{E}(x,y)e^{-jk_z z}$, where k_z is the propagation constant, (2.6) can be written as

$$F(\vec{E}) = \frac{1}{2} \iint\limits_{\Omega} \left[\frac{1}{\mu_r}(\nabla_t \times \vec{E}_t) \cdot (\nabla_t \times \vec{E}_t)^* - k_0^2 \epsilon_r \vec{E} \cdot \vec{E}^* \right. $$
$$\left. + \frac{1}{\mu_r}(\nabla_t E_z + jk_z \vec{E}_t) \cdot (\nabla_t E_z + jk_z \vec{E}_t)^* \right] d\Omega, \tag{2.7}$$

where ∇_t denotes the transverse curl operator, and $\vec{E}_t$ the transverse electric field. This formulation allows one to solve k_0, given a value of k_z. By solving for $k_z = 0$, ie. the cutoff wave numbers of the guide, and setting $E_z = 0$, the functional is simplified to

$$F(\vec{E}) = \frac{1}{2} \iint\limits_{\Omega} \left[\frac{1}{\mu_r}(\nabla_t \times \vec{E}_t) \cdot (\nabla_t \times \vec{E}_t)^* - k_0^2 \epsilon_r \vec{E}_t \cdot \vec{E}_t^* \right] d\Omega. \tag{2.8}$$

Having set $E_z = 0$, we are limited to solving the Transverse Electrical (TE) modes of a waveguide. By using the dual of the above functional, we may also solve the Transverse Magnetic (TM) modes of a waveguide. This limits the solution to, either homogeneous waveguides, or a limited number of loaded waveguide configurations.

Loaded waveguides which satisfy certain symmetry constraints [18] [19], have modes which are pure TE, or TM, modes. General inhomogeneous waveguides have, in addition to TE and TM modes, modes which contain both electric, and magnetic, longitudinal field components, simultaneously. Inhomogeneous waveguides are, however, not considered further.

2.1.3 Discretising the Domain

In order to apply the FEM, the domain must be discretised, and the field represented by basis functions defined on the individual elements.

Assuming the domain is discretised into M elements, within each element, e, the vector transverse field can be expanded as

$$\vec{E}_t^e = \sum_{i=1}^{n} \vec{W}_i^e E_{ti}^e = (\mathbf{W}^e)^T \mathbf{E_t^e}, \tag{2.9}$$

where n is the number of basis functions defined on the element, $\vec{W}_i^e$ is the ith basis function, and E_{ti}^e is the coefficient of the ith basis function. Substituting this expansion into (2.8), one obtains

$$F = \frac{1}{2} \sum_{e=1}^{M} \left([\mathbf{E}_t^e]^T \mathbf{S}^e [\mathbf{E}_t^e]^* - k_0^2 \epsilon_r [\mathbf{E}_t]^T \mathbf{T}^e [\mathbf{E}_t]^* \right), \tag{2.10}$$

where the elemental matrices are given by

$$S_{ij}^e = \frac{1}{\mu_r^e} \iint\limits_{\Omega^e} (\nabla_t \times \vec{W}_i^e) \cdot (\nabla_t \times \vec{W}_j^e)\, d\Omega, \qquad (2.11)$$

and

$$T_{ij}^e = \epsilon_r^e \iint\limits_{\Omega_e} \vec{W}_i \cdot \vec{W}_j\, d\Omega. \qquad (2.12)$$

Using global notation, (2.10) may be re-written as

$$F = \frac{1}{2}\mathbf{E}_t^T \mathbf{S}\mathbf{E}_t^* - \frac{1}{2}k_0^2\, \mathbf{E}_t^T \mathbf{T}\mathbf{E}_t^*. \qquad (2.13)$$

Applying the Ritz procedure[2], the generalised eigenvalue problem

$$\mathbf{S}\mathbf{E}_t = k_0^2\, \mathbf{T}\mathbf{E}_t \qquad (2.14)$$

is obtained. This may now be solved using linear algebra techniques.

2.2 Implementation of a 2D Vector FEM for Homogeneous Waveguides of Arbitrary Cross-section

The FEM, using the variational formulation described in the previous section, may now be applied to the problem of solving the modes, and mode cut-off wave-numbers, of a 2D, homogeneous wave guide, of arbitrary cross-section. The implementation of a FEM code is described, using basic, triangular Whitney (CT/LN) elements[2, §8]. The extension to higher order bases, and curved elements, are described in the following chapters.

2.2.1 Discretisation: Triangular Whitney Elements

Triangular elements are used to discretise the computational domain. Triangles are able to model any 2D, polygonal, domain exactly [20]. This property, and the fact that computer methods which automatically mesh such domains have long been known, has lent them wide-spread use in the CEM community[1].

The Whitney (CT/LN) basis functions used, constitutes the simplest vector basis applicable to triangular elements. It assigns a basis function, and hence degree of freedom, to each edge of the triangle. In simplex coordinates, the basis functions are given by

$$\begin{aligned}
\vec{W}_1 &= \lambda_1 \nabla\lambda_2 - \lambda_2 \nabla\lambda_1 \\
\vec{W}_2 &= \lambda_2 \nabla\lambda_3 - \lambda_3 \nabla\lambda_2 \\
\vec{W}_3 &= \lambda_1 \nabla\lambda_3 - \lambda_3 \nabla\lambda_1.
\end{aligned} \qquad (2.15)$$

The numbering convention is such that $\vec{W}_n$ is associated with an edge vector e_n, directed from node n to, node $n + 1 \mod 3$. The tangential field component, at the edge associated with $\vec{W}_n$, is directed along e_n.

At each edge of the element, each basis function has a zero tangential field component, except for the basis function assigned to the edge in question. Since the tangential field at each edge is constant, the degrees of freedom of an element, equate to the tangential field component, at each of the elements edges.

Tangential field continuity, or *curl* conformance, between two elements sharing an edge, is assured by assigning the same magnitude, and edge orientation, to the basis functions from both elements. Achieving this in practice, is discussed in the following subsection.

Integration of the elemental matrices may, at this point, be evaluated analytically. The resulting matrices may be found, for example, in [2, §8].

Decomposition of the computational domain into discrete elements, was achieved using the GRUMMP[21] 2D, and 3D, mesher.

2.2.2 Global Matrix Assembly and Solution

After the domain has been discretised, the contributions of the individual elements have to be assembled into the global **S** and **T** matrices, as used by (2.13).

In the case of scalar elements, this is simply achieved, by assigning the same variable to nodes shared by neighbouring elements. Vector elements, however, add the complication of the edge vector direction.

On a shared edge, the edge vectors of each element will lie on the same line. They might, however, be directed in opposite directions. When this occurs, the two basis functions will differ by a factor of -1.

This problem may solved in two ways. Either, by ensuring that all elements have consistent edge orientation, or by assuming a global edge orientation, and multiplying the applicable local matrix row and column by -1 if it differs[9].

The former method was implemented, by using a specific edge, and node, numbering convention within each triangle[22]. The nodes on the reference element, shown in Fig. 2.1, are chosen such that $A < B < C$, where A, B and C are the global numbers of the respective nodes. The edges are now defined so that they always point from lower, to higher numbered nodes. The edges are then $e_1 = \vec{AB}, e_2 = \vec{BC}, e_3 = \vec{AC}$.

Now it might be noted that the direction of e_3 is opposite to the definition of edge directions in the previous section. To take this into account, the negative of the third basis function must be used.

The global matrix assembly is now fairly straight forward. The elemental matrix entries are simply added to the global matrix rows/columns corresponding to edges e_1, e_2 and e_3. The global edge numbers were taken as
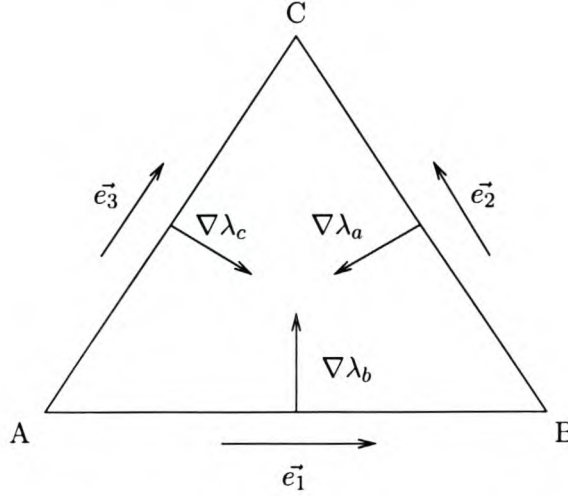
Figure 2.1: Reference Element

provided by the mesher.

The edge numbering supplied by the mesher is somewhat arbitrary, so it is likely that the edge numbers on a given triangle might be fairly widely spread. However, since a direct full matrix solver is used, there is no need to try and optimise the bandedness of the resulting global matrices.

The generalised eigen-system, posed in (2.13), is now solved using standard linear algebra routines. The resulting eigenvalues are the square of the cut-off wave number, for various modes of the waveguide. The eigenvectors represent the field distribution of a given mode, in terms of the basis functions used to discretise the computational domain.

In order to make full use of the FEM, sparse matrix techniques would typically be used. However, a direct solver is used, since it is desired to measure the effectiveness of the elements, and mappings, independently of other issues. Additionally, very few, if any, sparse eigen-solvers suitable for FEM CEM use, are currently publicly available.

The code was programmed in Python[23], using the Numerical Python[24] extension. Numerical Python provides, amongst other features, an efficient data array type, and an interface to the standard LAPACK[25] routines. LAPACK was set up to use the ATLAS[26] BLAS routines.

2.3 Conclusion

In this chapter, the finite element method was briefly described. The variational formulation used throughout this paper was presented, and discretisation of the computational domain discussed. Discussion of a basic FEM implementation using the above formulation and discretisation was presented.

Chapter 3

Curvilinear Coordinate Systems and Elements

This chapter discusses curvilinear coordinate systems, and how they may be used to define triangular, curved, curl conforming, vector elements. Unitary vectors are introduced, as the equivalent of unit vectors in standard, orthogonal, coordinates. Covariant-projection elements are defined as a means of mapping conventional elements to curved elements. Some practical issues, that affect the performance of curved elements, are discussed, followed by a description of how one might implement a curved element.

3.1   Literature Survey

The first real account of curved, vector, elements, as applied to the FEM in CEM, was by Crowley *et al.* [27]. His elements are, basically, extended scalar, interpolatory, quadrilateral and hexahedral, elements, with a Degree of Freedom (DOF) for each dimension of the element at each node, and were dubbed covariant projection elements. They are also discussed in [1, §7.6].

The chief contribution, is the use of the unitary vectors (discussed in the following sections), which are local to each element, rather than the conventional Cartesian unit vectors, in the definition of basis functions. Since unitary vectors define vectors tangential to element edges, this allows both mixed order basis functions, and curl conformance, to be built into these elements.

These elements may then be considered as proper vector, edge elements, and do indeed eliminate spurious solutions. In [27], the inclusion condition is postulated as a sufficient condition for the elimination of spurious solutions. It is also stated that these elements satisfy the inclusion condition. However, it has since been shown that covariant projection elements do not satisfy the inclusion condition [28].

Several researchers have applied these elements to different CEM prob-

lems [29], [30], [31], [32], [33]. The first two papers also describe some aspects of the derivation of the elements that are not discussed in [27]. They all found these elements to be effective, producing spurious solutions in only one specific case [30]. In [30], these elements were found to be adept at modelling singularities. When full-order basis functions were used with a loaded waveguide, spurious modes were however encountered. Mixed-order elements did not exhibit spurious modes.

In [34], Wang and Ida introduce elements which are generalised forms of the elements described in [15]. Their methodology is applied to hexahedral, and tetrahedral, elements. Their higher order elements are also interpolatory.

The paper by Graglia *et al.* [8], which is ostensibly about higher order interpolatory bases, additionally provides a fair amount of detail pertaining to the application of curvilinear elements in an appendix. This paper could be seen as a generalisation of Crowley's work mentioned above.

The elements of Graglia *et al.* in curvilinear form are used by [35] and [36]. The former paper uses these elements in the context of implementing a curved, perfectly matched, layer. The latter paper mentions curved elements in passing, and is mainly focused on a special, efficient, FEM technique for calculating the scattering from deep cavities.

In [37] the application of covariant projection mapping is explained quite succinctly. It shows all the required definitions for mapping between an arbitrary reference coordinate system, and Cartesian coordinates. Furthermore, the curl operator in the reference coordinates is derived, and it is shown how the typical FEM elemental matrices may be formulated using these results.

3.2   Theory

In order to use a given finite element, one has to be able to determine the entries of the $\mathbf{S}$ and $\mathbf{T}$ elemental matrices. Furthermore, the element has to have the right kind of continuity, in order to be compatible with other elements in a mesh, and to allow an accurate solution to be obtained.

In this section, the theory neccesary to assemble the $\mathbf{S}$, and $\mathbf{T}$, matrices for a curved element is discussed. The element may be of arbitrary shape, using arbitrary basis functions, defined in terms of the reference coordinates, (u, v).

The derivation is done in 2D here, in order to keep it as simple as possible. Application to three dimensional coordinates is similar, with the main difference being the size of the Jacobian, and a more complicated expression for the vector operators.

Specific mappings, continuity conditions, and compatibility with other elements will be further discussed in chapter 5.

3.2.1 Introduction of the Reference Coordinates

A reference cell, described in (u, v) coordinates, will be mapped onto physical (x, y) space, to yield an element of the desired shape. We can map from $(u, v) \rightarrow (x, y)$ by making formulas

$$
\begin{aligned}
x &= x(u, v) \\
y &= y(u, v),
\end{aligned}
\tag{3.1}
$$

and inverting the relation to obtain $(x, y) \rightarrow (u, v)$:

$$
\begin{aligned}
u &= u(x, y) \\
v &= v(x, y).
\end{aligned}
\tag{3.2}
$$

The mapping is shown graphically in Fig. 3.1
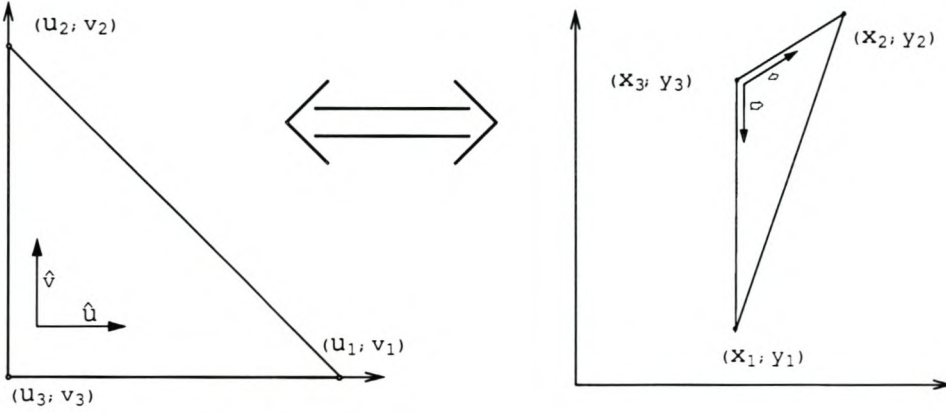
Figure 3.1: Reference (u, v) triangle mapped to (x, y) triangle

3.2.2 Change of Coordinates in the Integrand

In the case of a FEM solution, functions, W_{mn}, have to be integrated over the area of the element in real, geometric (x, y) space. Given an integral defined in (x, y),

$$
\begin{aligned}
I &= \iint_A W_{mn}(x, y) dA \\
&= \iint_A W_{mn}(x, y) dx dy,
\end{aligned}
\tag{3.3}
$$

it may be integrated in (u, v) using the Jacobian of the coordinate transform [38, §8.17]:

$$
I = \iint_A W_{mn}(u, v) \det(\mathbf{J}) du dv
\tag{3.4}
$$

There are some restrictions, mainly that the determinant should never be zero, and the transformation be one to one, over the domain of interest.

The Jacobian matrix of the transformation $\Im$, from $(x, y) \rightarrow (u, v)$ is defined as

$$\mathbf{J}(\Im) = \begin{bmatrix} \frac{\delta x}{\delta u} & \frac{\delta y}{\delta u} \\ \frac{\delta x}{\delta v} & \frac{\delta y}{\delta v} \end{bmatrix}, \text{ or}$$

$$\mathbf{J}(\Im) = \left[\frac{\delta(x,y)}{\delta(u,v)} \right]. \tag{3.5}$$

The Jacobian itself, is $\det(\mathbf{J})$. A Jacobian matrix for the inverse transformation, $\Im^{-1}$, from $(u, v) \rightarrow (x, y)$, may be defined as

$$\mathbf{J}(\Im^{-1}) = \begin{bmatrix} \frac{\delta u}{\delta x} & \frac{\delta v}{\delta x} \\ \frac{\delta u}{\delta y} & \frac{\delta v}{\delta y} \end{bmatrix}, \text{ or}$$

$$\mathbf{J}(\Im^{-1}) = \left[\frac{\delta(u,v)}{\delta(x,y)} \right]. \tag{3.6}$$

Fortunately [1, P. 280],

$$\mathbf{J}(\Im^{-1}) = \mathbf{J}^{-1}(\Im). \tag{3.7}$$

This means that, irrespective of which transformation's Jacobian is most convenient to determine, the inverse Jacobian at a given point can be determined by numeric inversion.

Once the Jacobian matrix is known, the integration can be performed fairly simply when one is dealing with scalar functions. Vector valued functions are somewhat more complex, since the vector direction senses need to be taken into account.

3.2.3 Curvilinear (General) Coordinates

In order to make sense of vector quantities across the coordinate transformation, *general* or *curvilinear* coordinates are needed, as show by Stratton[39]. Defining $\vec{r}$ as the vector from an arbitrary origin, to a variable point $P(x, y)$, *unitary vectors*, are defined as

$$\vec{a}_u = \frac{\delta \vec{r}}{\delta u}$$

$$\vec{a}_v = \frac{\delta \vec{r}}{\delta v}. \tag{3.8}$$

Reciprocal unitary vectors are, in turn, defined as

$$\vec{a}^u = \frac{1}{A}(\vec{a}_v \times \hat{z})$$

$$\vec{a}^v = \frac{1}{A}(\hat{z} \times \vec{a}_u), \tag{3.9}$$

where $A = \hat{z} \cdot (\vec{a}_u \times \vec{a}_v)$. Similarly, the unitary vectors may be defined in term of the reciprocal unitary vectors

$$
\begin{aligned}
\vec{a}_u &= \frac{1}{A}(\vec{a}^v \times \hat{z}) \\
\vec{a}_v &= \frac{1}{A}(\hat{z} \times \vec{a}^u).
\end{aligned}
\tag{3.10}
$$

The unitary, and reciprocal unitary vectors are bi-orthogonal:

$$
\vec{a}^\xi \cdot \vec{a}_\eta = \delta_{\xi\eta}.
\tag{3.11}
$$

Using these properties, any vector quantity $\vec{W}$ may now be expressed in curvilinear coordinates as

$$
\vec{W} = (\vec{W} \cdot \vec{a}_u)\vec{a}^u + (\vec{W} \cdot \vec{a}_v)\vec{a}^v
\tag{3.12}
$$

or

$$
\vec{W} = (\vec{W} \cdot \vec{a}^u)\vec{a}_u + (\vec{W} \cdot \vec{a}^v)\vec{a}_v.
\tag{3.13}
$$

$(\vec{W} \cdot \vec{a}_{u,v})$ and $(\vec{W} \cdot \vec{a}^{u,v})$ are referred to as, respectively, the *covariant* and *contravariant* components of the vector $\vec{W}$.

When (x, y) refer to Cartesian coordinates, (3.8) and (3.9) may be written as[37]

$$
\begin{aligned}
\vec{a}_u &= \frac{\delta x}{\delta u}\hat{x} + \frac{\delta y}{\delta u}\hat{y} \\
\vec{a}_v &= \frac{\delta x}{\delta v}\hat{x} + \frac{\delta y}{\delta v}\hat{y}
\end{aligned}
\tag{3.14}
$$

and

$$
\begin{aligned}
\vec{a}^u &= \nabla u \\
\vec{a}^v &= \nabla v.
\end{aligned}
\tag{3.15}
$$

3.2.4 Mapping the Element: Covariant Projection Mapping

Since the elements are required to be curl-conforming, one has to be able to ensure tangential continuity of basis functions at the edges of an element. Looking again at (3.14) and (3.15), we see that unitary vectors are directed along lines of constant coordinate (ie. $\vec{a}_u$ points in the direction of constant v), while the reciprocal unitary vectors point in the direction of steepest reference coordinate ascent, in physical coordinates.

Since the tangents of the reference triangle edges lie along lines of constant u, v, or $(u + v)$, the unitary vectors represent tangents at the edges.

Conversely, the reciprocal unitary vectors represent normals, due to the bi-orthogonality property (3.11).

By defining the basis functions in terms of their covariant component projections, the tangential continuity properties they possess on the reference element, will be maintained once they are mapped to (x, y) coordinates.

To see this, consider the bottom edge of the reference triangle. This edge is represented by constant $v = 0$. Since $\vec{a}_u$ is directed along lines of constant v, it is thus tangential to the edge $v = 0$. Since the u covariant component of $\vec{W}$ is $W_u = (\vec{W} \cdot \vec{a}_u)$, it represents the component of $\vec{W}$ tangential to the bottom edge of the reference triangle, in both reference, and physical, coordinates. Fig. 3.2 shows lines of constant coordinate.
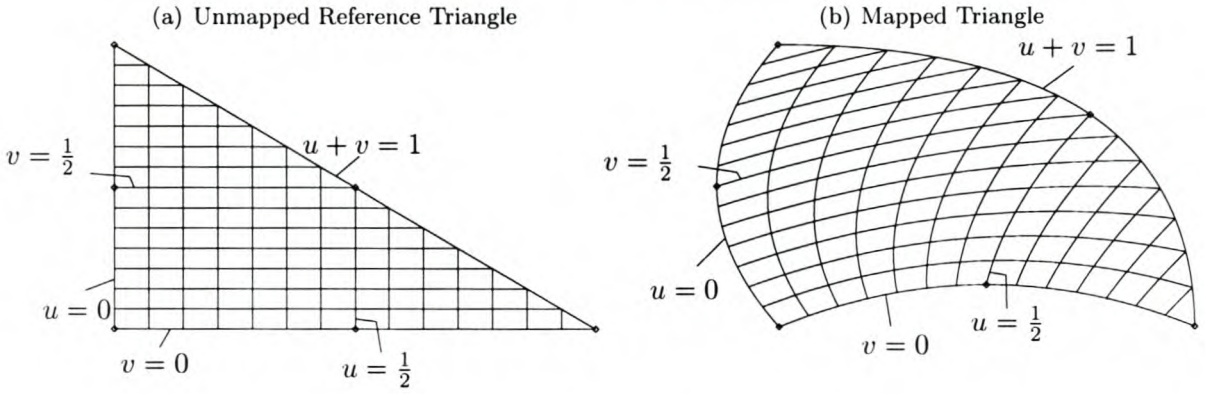
Figure 3.2: Lines of Constant Coordinate

Similarly, defining basis functions in terms of their contravariant components, normal continuity properties are preserved. In the former case, the resultant mapping will be useful for applications that require curl-conforming elements, such as the FEM under consideration in this document. In the latter case, divergence conforming elements may be constructed, for use in, eg. Method of Moments [8] [40].

Since covariant components will henceforth be used to represent vector basis functions in the reference coordinates, it is convenient to redefine (3.15) as

$$\hat{u} = \nabla u$$
$$\hat{v} = \nabla v. \tag{3.16}$$

Consistent with the above convention, the covariant components of a vector, $\vec{W}$, can be defined as

$$W_u = (\vec{W} \cdot \vec{a}_u)$$
$$W_v = (\vec{W} \cdot \vec{a}_v). \tag{3.17}$$

Noting the relation between (3.14) and the Jacobian matrix, we may now write

$$\begin{bmatrix} W_x \\ W_y \end{bmatrix} = \mathbf{J}^{-1} \begin{bmatrix} W_u \\ W_v \end{bmatrix}, \qquad (3.18)$$

and similarly

$$\begin{bmatrix} \frac{\delta}{\delta x} \\ \frac{\delta}{\delta y} \end{bmatrix} = \mathbf{J}^{-1} \begin{bmatrix} \frac{\delta}{\delta u} \\ \frac{\delta}{\delta v} \end{bmatrix}. \qquad (3.19)$$

The curl operator is needed in order to evaluate the elemental matrices. Using (3.18) and (3.19), and taking the analytical inverse of $\mathbf{J}$, the curl operator may be expressed using only covariant components and their derivatives in (u, v):

$$\hat{z} \cdot \nabla \times \vec{W} = \left[\frac{\delta W_y}{\delta x} - \frac{\delta W_x}{\delta y} \right] = \frac{1}{\det(\mathbf{J})} \left[\frac{\delta W_v}{\delta u} - \frac{\delta W_u}{\delta v} \right]. \qquad (3.20)$$

3.2.5 Evaluation of the Elemental Matrices

Using (3.20), we can now write the integrals for the $\mathbf{S}$ and $\mathbf{T}$ matrices completely in terms of (u, v) [37]:

$$\mathbf{S} = \iint_A \nabla \times \vec{W}_m \cdot \nabla \times \vec{W}_n \, dxdy$$

$$= \int_0^1 \int_0^{1-u} \frac{1}{\det(\mathbf{J})} \left[\frac{\delta W_{m(v)}}{\delta u} - \frac{\delta W_{m(u)}}{\delta v} \right] \left[\frac{\delta W_{n(v)}}{\delta u} - \frac{\delta W_{n(u)}}{\delta v} \right] dvdu \qquad (3.21)$$

and

$$\mathbf{T} = \iint_A \vec{W}_m \cdot \vec{W}_n \, dxdy = \iint_A \begin{bmatrix} W_{m(x)} & W_{m(y)} \end{bmatrix} \begin{bmatrix} W_{n(x)} \\ W_{n(y)} \end{bmatrix} dxdy$$

$$= \int_0^1 \int_0^{1-u} \begin{bmatrix} W_{m(u)} & W_{m(v)} \end{bmatrix} \mathbf{J}^{-T} \mathbf{J}^{-1} \begin{bmatrix} W_{n(u)} \\ W_{n(v)} \end{bmatrix} \det(\mathbf{J}) dvdu, \qquad (3.22)$$

where W_n represents the nth basis function, and $W_{n(x)}$ the $\hat{x}$ component of the same function.

This means that, in order to perform a coordinate mapping, we need:

- functions with continuous partial derivatives, forming a one to one mapping $(u, v) \rightarrow (x, y)$, or vice versa,

- an expression for $\mathbf{J}$, or $\mathbf{J}^{-1}$ in terms of (u, v),

- the required partial derivatives of the covariant components of the basis functions in terms of (u, v).

3.3 Application of Covariant Mapping to Elements Defined in Simplex Coordinates

Triangular vector basis functions are typically expressed in term of simplex coordinates, and the gradient of simplex coordinates. Taking, for example, the Whitney basis

$$\vec{W}_1 = \lambda_1 \nabla \lambda_2 - \lambda_2 \nabla \lambda_1$$
$$\vec{W}_2 = \lambda_2 \nabla \lambda_3 - \lambda_3 \nabla \lambda_2 \qquad (3.23)$$
$$\vec{W}_3 = \lambda_1 \nabla \lambda_3 - \lambda_3 \nabla \lambda_1,$$

it now has to be cast into a form amenable to being mapped. Defining

$$u = \lambda_1$$
$$v = \lambda_2, \qquad (3.24)$$

and using the linear dependence of λ_3 on λ_1 and λ_2,

$$\lambda_3 = 1 - \lambda_1 - \lambda_2 = 1 - u - v, \qquad (3.25)$$

we see that casting (3.23) into covariant components is surprisingly simple, since (3.16) show us that $\nabla \lambda_1 = \hat{u}, \nabla \lambda_2 = \hat{v}$ and $\nabla \lambda_3 = -(\hat{u} + \hat{v})$.

Writing (3.23) in covariant components, we now have:

$$\vec{W}_1 = -v\hat{u} + u\hat{v}$$
$$\vec{W}_2 = -v\hat{u} + (u-1)\hat{v} \qquad (3.26)$$
$$\vec{W}_3 = (v-1)\hat{u} - u\hat{v}.$$

Casting any basis defined in terms of simplex coordinates and their gradients into covariant components, is easily achieved using this process.

In addition to the basis functions in covariant components, some derivatives are needed to evaluate the curl operator. From (3.20) we see that the partial derivatives

$$\frac{\delta W_{n(v)}}{\delta u} \text{ and } \frac{\delta W_{n(u)}}{\delta v}$$

are also needed.

3.4 Basis Function Distortion

Applying a non-linear mapping to a basis will inevitably result in some level of distortion. Even a polynomial mapping will cause the basis function to be non-polynomial, since rational polynomial functions will be involved in the Jacobian.

When polynomial basis functions are mapped, they will no longer span the expected polynomial space (see §4.2). Rather, one could say that [8], if pth order basis functions are defined on the reference element, the resulting basis in real space is complete to order p, with respect to $\hat{n}/\det(\mathbf{J})$ as a weighting factor.

In [5, §8.3, §13.3] it is qualitatively shown how distortion from the original element shape affects the basis function. A highly distorted basis function could become non-sensical. Avoiding this essentially entails ensuring that the mapping remains one to one, and that the Jacobian is non-vanishing.

Supposing that the mapping is one to one, and has a non-vanishing Jacobian, it is desirable to know how element distortion affects the accuracy of a solution. In [12] it is shown how distorted basis functions can affect solution accuracy negatively. They do, however, take the rather extreme example of a parallel plate capacitor meshed with two triangular, linear elements. The elements used are able to obtain an exact solution when undistorted. This is discussed further in §5.3.

Another issue potentially affecting accuracy, independent of the distorted basis functions ability to model the required field, exists. When an element is highly distorted, vectors which would have been orthogonal on the reference element, might be close to co-linear once mapped. This could result in poor matrix conditioning.

3.5 Conclusion

In this chapter, a survey of the electronic engineering literature concerning the FEM in curved domains was presented. Coordinates for a reference triangle were introduced. Integration over the reference triangle was described in terms of the Jacobian of a coordinate transform. Curvilinear coordinates were described, along with the covariant projection mapping, which allows tangential continuity to be proscribed in real, as well as reference, coordinates. Evaluation of the FEM elemental matrices in reference coordinates were described. It was shown how, simply, basis functions defined in terms of simplex elements may be mapped onto curved shapes. The effect of curvilinear mappings on basis function performance was briefly discussed.

Chapter 4

Higher Order FEM Basis Functions

This chapter discusses the theory behind, and implementation of, higher order, vector elements for the FEM. Some theoretical aspects of polynomial vector bases, and how they affect solution efficiency are discussed. The automation of the derivations needed to implement Webb's [9] basis functions of arbitrary order is described for triangular elements. Finally, practical implementation of such basis functions is described.

4.1 Element Requirements

An element used to discretise a domain for the FEM, needs to fulfil certain requirements. The basis functions defined on the element should approximate the physical field well. Certain inter-element continuity conditions should also be taken into account. The physical shape of the element should be able to fit the geometry of the problem well, though this is covered in chapter 3.

4.1.1 Elemental Approximation Efficiency

An efficient element would be one that provides a good level of approximation per DOF used in its representation. Computational cost is largely proportional to the number of DOFs, so an efficient element will obviously be desirable.

The good ability of higher-order, piecewise-polynomial functions to fit arbitrary functions is well known [2]. In general, piecewise-polynomial approximations' efficiency improve with increasing polynomial order, but the exact rate of convergence depends on the nature of the differential equation being solved [5].

24

4.1.2 Continuity Conditions

Accurate modelling of the field in an inhomogeneous domain therefore requires that tangential-, but not normal continuity be enforced between elements. This is further discussed in §4.3.3.

Enforcing continuity of any kind between different elements, requires that they are compatible. Considering tangential continuity, this means that the tangential field on an edge, should be determined only by parameters on the edge itself.

In other words, the interior configuration of an element, should have no effect on the tangential field on element edges. Furthermore, given the same set of edge parameters, both elements should have the same tangential field along the common edge.

4.2 Polynomial Vector Function Spaces

The discussion of function spaces is limited to the 2D case here. The extension to 3D is similar, and is discussed, along with 1D and 2D spaces, in [9].

4.2.1 1D Vector Polynomial Spaces

We define vector polynomials on a 1D simplex, using the variables λ_1, λ_2, where $\lambda_1 + \lambda_2 = 1$, $\lambda_1 = 0$ at node 1, and similarly $\lambda_2 = 0$ at node 2. We define V_p as the set of all polynomials of at most degree p in λ_1 and λ_2. The dimension of V_p is $p + 1$, the same as the number of linearly independent scalar polynomials of degree p.

Any function in V_p may be written in the form

$$P_1(\lambda_1, \lambda_2)\lambda_1 \nabla \lambda_1 + P_2(\lambda_1, \lambda_2)\lambda_2 \nabla \lambda_2. \tag{4.1}$$

Here P_1 and P_2 are polynomials of degree $p - 1$, and $\nabla = \hat{x}\frac{\delta}{\delta x}$.

V_p may be split into the subspaces, G_p and W_p. G_p contains all the vector functions that are the gradients of scalars polynomials of order $p + 1$ that vanish at both nodes. There are p such scalar polynomials, so the dimension of G_p is p. This leaves the subspace W_p with a dimension of 1. A basis for W_p is given by

$$\lambda_1 \nabla \lambda_2 - \lambda_2 \nabla \lambda_1. \tag{4.2}$$

It can be seen that W_p coves a space identical to the original Whitney basis.

4.2.2 2D Vector Polynomial Spaces

Now we define vector polynomials on the triangular 2D simplex. The standard 2D simplex coordinates, λ_1, λ_2 and λ_3, as defined in eg. [1] are used. Now, at node n, $\lambda_n = 1$, and at the edge opposite node n, $\lambda_n = 0$.

V_p is defined as the space of all 2D polynomial vector functions of degree p or less. There are $(p+1)(p+2)/2$ linearly independent scalar polynomials in 2D. Hence, there are $(p+1)(p+2)$ 2D vector valued polynomials functions, and the dimension of V_p is therefore also $(p+1)(p+2)$.

Taking a basis function from the 1D V_p space, written in the form (4.1), as a 2D vector function, it has the following properties:

- its tangential component vanishes on the edges $\lambda_1 = 0$ and $\lambda_2 = 0$ (due to $\nabla\lambda_i$ being perpendicular to the edge $\lambda_i = 0$)

- its tangential component on the edge $\lambda_3 = 0$ is identical to the 1D basis function.

The second property ensures that the 2D functions generated in this way are linearly independent. A 1D basis taken into 2D space thus forms a subspace of V_p, of dimension $p + 1$, now defined to be the edge space $V_p^{(e)}$. $V_p^{(e)}$ may be subdivided into $W_p^{(e)}$ and $G_p(e)$ as in §4.2.1.

By permuting the variable subscripts of $V_p^{(e)}$ through $(1 \to 2 \to 3 \to 1)$, two similar edge spaces may be obtained. The combination of these three spaces will be referred to as $3V_p^{(e)}$.

The rest of V_p is made up of polynomial vector functions, of degree no more than p, with vanishing tangential components at all the edges. Since these functions are not associated with any edges, they are dubbed, face functions, and the subspace containing them, defined as $V_p^{(f)}$.

Functions in $V_p^{(f)}$ may be written as

$$\lambda_1\lambda_2 P_3(\lambda_1, \lambda_2, \lambda_3)\nabla\lambda_3 + \lambda_2\lambda_3 P_1(\lambda_1, \lambda_2, \lambda_3)\nabla\lambda_1$$
$$+ \lambda_3\lambda_1 P_2(\lambda_1, \lambda_2, \lambda_3)\nabla\lambda_2, \quad (4.3)$$

where P_1, P_2 and P_3 are polynomials of degree $p - 2$. $V_p^{(f)}$ has dimension $(p-1)(p+1)$. Similar to the $V_p^{(e)}$ split, we can partition $V_p^{(f)}$ into subspaces $G_p^{(f)}$ and $R_p^{(f)}$.

Let $G_p^{(f)}$ be the subspace of $V_p^{(f)}$ containing functions that are the gradient of scalar polynomials of degree $p + 1$. Since there are $p(p - 1)/2$ such functions, the dimension of $G_p(f)$ is $p(p - 1)/2$. Functions in $G_p^{(f)}$ may be written in the form

$$\nabla(\lambda_1\lambda_2\lambda_3 P(\lambda_1, \lambda_2, \lambda_3)), \qquad (4.4)$$

where P is a polynomial of degree $p - 2$. Since there are $p(p - 1)/2$ such polynomials, $G_p^{(f)}$ has dimension $p(p - 1)/2$.

The remaining functions of $V_p^{(f)}$ then belong to $R_p^{(f)}$. Since no functions in $R_p^{(f)}$ may be written as the gradient of a scalar, they must all have non-zero curl. Thus, $R_p^{(f)}$ is the space of *rotational* functions. The dimension of this space is $(p - 1)(p + 2)/2$.

While $G_p^{(f)}$ and $R_p^{(f)}$ split the face functions into gradient, and rotational subspaces, the same is not quite true for $3G_p^{(e)}$ and $3W_p^{(e)}$. While $3G_p^{(e)}$ certainly contains only gradient functions, $3W_p^{(e)}$ spans a space containing a rotational function, and the two constant functions, which are gradients.

4.3 Basis Efficiency Considerations

4.3.1 Expected Convergence Rate vs. Basis Order

A field approximated by a polynomial may be considered as a pth order truncated Taylor series of the true field. A truncated Taylor series expansion, of a function f, expanded around a, is given by

$$f(x) = \sum_{k=0}^{n} \frac{f^{(k)}(a)}{k!}(x - a) + R_p(x). \qquad (4.5)$$

$R_p(x)$ is the remainder of order p. The remainder is bounded as

$$|R_p(x)| < M\frac{|x - a|^{p+1}}{(p + 1)!}, \qquad (4.6)$$

where M is a positive constant such that $|f^{(p+1)}(t)| < M$ for all t such that $|t - a| \leq |x - a|$.

It is clear that $|x - a|$ is directly proportional to the maximum mesh edge size, h. The order of the approximation error made by a pth order base, is thus given by $O(h^{(p+1)})$. A similar result applies in the case of a multivariate polynomial, where p is the highest full order of the approximating polynomial [41].

Looking at the functional used to solve the vector Helmholtz equation (2.8), repeated here for convenience,

$$F(\vec{E}) = \frac{1}{2} \iint_{\Omega} \left[\frac{1}{\mu_r}(\nabla_t \times \vec{E}_t) \cdot (\nabla_t \times \vec{E}_t)^* - k_0^2 \epsilon_r \vec{E}_t \cdot \vec{E}_t^* \right] d\Omega, \qquad (4.7)$$

it can be seen that the field, as well as the curl of the field, is involved. Since curl is a derivative operator, taking the curl of a polynomial will reduce its order. The full order of curl approximated by a pth order base is therefore $p - 1$.

A field represented by a polynomial vector basis of order p, clearly has a curl approximation of the field that will no longer be of full order. The curl approximation will therefore converge as $O(h^p)$.

In microwave problems, the importance of the curl of a field is typically as important as the field itself. The result is that the functional convergence is dominated by the convergence of the curl. Since the functional contains the square of the curl, the resultant convergence is as $O(h^{2p})$.

27

4.3.2 Mixed Order Bases

In §4.2.2 it was shown that a basis may be split into a subspace representing gradient functions, which have zero curl, $3G_p^{(e)} \oplus G_p^{(f)}$, a subspace of rotational face functions, $R_p^{(f)}$, and the original Whitney base $3W_p^{(e)}$. Since the gradient functions do not contribute to the curl, some of them may be removed, provided the resulting approximation is still complete to order $p - 1$.

While the number of DOFs have been reduced, the integrand of the functional is still complete to order $p - 1$. Thus, the asymptotic convergence rate is the same as for the full order element. Bases which has had the highest order gradient DOFs removed, are referred to as mixed-order, or reduced, bases.

The former name is after the fact that, on the edges of an element, these bases will interpolate the tangential, and normal, field components to different orders. This can be seen from the fact that, barring $3W_p^{(e)}$, all the edge functions are gradient functions. Furthermore, the functions in $G_p^{(f)}$ vanishes at all the edges of an element.

Thus, at the edges, the only field contributions come from the edge functions, and the rotational face functions. Since the edge functions are of reduced order, and are the only functions that contribute to the tangential field at the edges, it is clear that the tangential field component will be of reduced order, relative to the normal component.

While mixed order elements result in the same rate of convergence as full order elements, there are situations where its beneficial to use full order elements. This happens when, in the domain being modelled, the curl of a field is significantly less important than the field itself [9]. In the electro-quasistatic limit, the curl will be of vanishing importance. Similarly, using the dual (ie $\vec{H}$) formulation, in the magnetoquasistatic limit.

4.3.3 Spurious Modal Solutions

Spurious modal solutions were the bane of early CEM FEM work. The introduction of vector elements, seems to have made them a thing of the past.

To see why, consider that $\vec{E}$ and $\vec{H}$ fields are not necessarily continuous everywhere. A discontinuity in the physical properties of a domain, results in discontinuity in the field components, normal to the boundary of the physical discontinuity.

At first glance, this would seem to intimate that full continuity should be enforced in homogeneous regions, but this is not true. Qualitatively speaking, one might imagine the border between each element being a discontinuity, due to the imperfect modelling of the field on each element.

When the FEM was initially applied to vector CEM problems, elements with full continuity were used. As mentioned earlier, this is physically incorrect in inhomogeneous domains.

Spurious modes in homogeneous domains require a slightly more complex explanation. The vector Helmholtz equation for a source free homogeneous region (2.4) is

$$\nabla \times \left(\frac{1}{\mu_r} \nabla \times \vec{E} \right) - k_o^2 \epsilon_r \vec{E} = 0 \quad \text{in } \Omega. \tag{4.8}$$

Solutions of (4.8) represent fields that may be split into two categories [37],

1. valid electromagnetic fields, of the form $\vec{E} = \nabla \times \vec{V}$, where V is proportional to the magnetic field $\vec{H}$

2. $\vec{E} = \nabla \Phi$.

Solutions of the second kind are valid solutions of (4.8) in the case of $k_0 = 0$, since $\nabla \times \nabla \Phi = 0$, but do not represent physical solutions of an electromagnetic field in a source free region. Solutions of this form are said to form the null-space of the curl-curl operator.

Since the non-physical solutions correspond to zero eigenvalues, they should be easy to tell apart from the physical solutions. Enforcing full inter-element continuity, however, distorts the modelling of this null-space to such an extent, that the computed eigenvalues of this space is of the same magnitude as the eigenvalues corresponding to physical solutions [37] [8].

Sometimes, however, this is not enough. Further precautions are neccesary for brick elements [37]. In [30], spurious modes were encountered when using full order quadrilateral covariant-projection elements.

In [42], a somewhat dissenting view is taken by Mur. He takes to task the belief that edge elements are panacea. An alternative element is also proposed in [43]. While edge elements do have their limitations, it is clear, all the same, that they work much better than what was available before.

4.4 Implementation of Arbitrary Order Basis Functions using a CAS

Hierarchal vector basis functions were chosen for implementation, since they would involve less work for each additional order of base, than using interpolatory bases.

In [9], explicit formulas are given for hierarchal basis functions of arbitrary order. Manually expanding these formulas into a form suitable for computation would be very tedious, and error prone, especially for higher order bases. For this reason, they were implemented using the Maxima [44] Computer Algebra System (CAS).

4.4.1 Expansion of the Edge Basis Functions $G_p^{(e)}$

The 1D gradient space G_p requires p basis functions. Increasing the order from $p-1$ to p, thus requires 1 extra basis function.

The 2D edge gradient space $G_p^{(e)}$ may be obtained by cyclic permutation of the variables subscripts. Increasing the order from $p-1$ to p will therefore result in 3 additional basis functions.

The additional function required for order p is given by

$$\vec{G}_p^{(e)} = \nabla(\lambda_1 \lambda_2 (\lambda_1 - \lambda_2)^{p-1}). \tag{4.9}$$

In the CAS system, (u, v) is substituted for (λ_1, λ_2). The ∇ operator is applied by using the CAS systems' total derivative function. The result is then in terms of u, v and $\nabla u, \nabla v$, which is exactly what is required.

The basis function for the first edge has now been obtained. Obtaining the remaining two edge functions is easily managed by substitution. By applying the substitution $u = v, v = w, w = u$ twice, the basis function pertaining to edge two, and three, are obtained in order. These functions are then simplified by the substitution $w = (1-u-v)$ and $\nabla w = -(\nabla u + \nabla v)$.

4.4.2 Face Function Triplets

The face functions below, are defined in terms of triplets of a scalar function, F_{pi}. This function generates τ triplets of order p, where $\tau = \text{floor}(p/3)$. The first function of the ith triplet is

$$F_{pi} = (\lambda_1 \lambda_2 \lambda_3)^i \lambda_1 \lambda_2 (\lambda_1 - \lambda_2)^{(p-3i-2)}, \qquad i = 1, \dots, \tau - 1 \tag{4.10}$$

and

$$F_{p\tau} = \begin{cases} (\lambda_1 \lambda_2 \lambda_3)^\tau, & \text{if } p \bmod 3 = 0 \\ (\lambda_1 \lambda_2 \lambda_3)^\tau (\lambda_1 - \lambda_2), & \text{if } p \bmod 3 = 1 \\ (\lambda_1 \lambda_2 \lambda_3)^\tau \lambda_1 \lambda_2, & \text{if } p \bmod 3 = 2. \end{cases} \tag{4.11}$$

When $p \bmod 3 = 0$, all three functions in the τth triplet are identical, thus only one must be used. When $p \bmod 3 = 1$, there are only two linearly independent functions in the τth triplet, thus only two must be used. Lastly, $p \bmod 3 = 2$ results in three independent equations. In total, each F_{pi} generates $(p-2)$ new scalar polynomials.

4.4.3 Expansion of the Face Basis Functions $\vec{G}_p^{(f)}$ and $\vec{R}_p^{(f)}$

The first function in the ith triplet of gradient face functions is given by

$$\vec{G}_{pi}^{(f)} = \nabla F_{p+1, i+1}, \qquad i = 0, \dots, \text{floor}\left(\frac{p+1}{3}\right) - 1. \tag{4.12}$$

Since we are using F_{p+1}, the required $(p-1)$ new basis functions are generated, going from order $p-1$ to p.

The first function in the ith triplet of rotational face functions are given by

$$\vec{R}_{pi}^{(f)} = F_{pi}\nabla\lambda_3, \qquad i = 0, \ldots, \sigma - 1, \tag{4.13}$$

where $\sigma = \text{floor}(\frac{p-1}{3})$ ((4.10) extended to include the case $i = 0$) and

$$\vec{R}_{p\sigma}^{(f)} = \begin{cases} (F_{p\sigma})\nabla\lambda_3 & \text{if } p \bmod 3 = 0 \\ (\lambda_1\lambda_2\lambda_3)^{\sigma}[(\lambda_1 - \lambda_2)\nabla\lambda_3 & \\ \quad + (\lambda_2 - \lambda_3)\nabla\lambda_3 + (\lambda_3 - \lambda_1)\nabla\lambda_2] & \text{if } p \bmod 3 = 1 \\ (\lambda_1\lambda_2\lambda_3)^{\sigma}[-2\lambda_1\lambda_2\nabla\lambda_3 & \\ \quad + \lambda_2\lambda_3\nabla\lambda_1 + \lambda_3\lambda_1\nabla\lambda_2] & \text{if } p \bmod 3 = 2. \end{cases} \tag{4.14}$$

When $p \bmod 3$ is respectively one and two, the σth triplet consists of, respectively, one and two distinct functions. This results in the required p additional basis functions, when going from order $p-1$ to p.

The substitution $u = \lambda_1, v = \lambda_2, w = \lambda_3$ was made. As in §4.4.1, the variables were permuted, and the correct substitutions for w and ∇w were made.

When these equations are programmed, the right number of equations must be discarded from the last triplet. In the case of tetrahedral elements, it would have been slightly more complicated than just throwing a number of functions away, since the tangential components on faces would also have to match.

4.4.4   Even and Odd Basis Function Symmetry

One of the requirements on our elements was that they should be able to enforce tangential continuity. As was seen in §2.2.2, the relative orientation of a shared edge affects the sign of the basis function along this edge.

Generally speaking, the edge functions used here have either even or odd symmetry under exchange of their edge variables. Those that have odd symmetry, such as the Whitney base, require under the edge orientation scheme used here, that the sign of every function corresponding to the third edge of a given triangle, be inverted. Functions that have even symmetry, may be left unchanged.

The edge functions $\vec{G}_p^{(e)}$ have even symmetry when $p \bmod 2 = 1$, and odd symmetry when $p \bmod 2 = 0$. It is thus easy to determine when a function needs to be negated.

4.5 Conclusion

This chapter, in general discussed higher order basis functions, and their implementation. Desirable qualities for an element to possess were discussed. The polynomial spaces covered by the bases here considered were discussed. The order of base, and the continuity conditions enforced over the elements used were discussed w.r.t. solution efficiency, and spurious modes. The implementation of arbitrary order bases, derived from the general basis function equations of Webb, using a CAS, was described.

Chapter 5

Coordinate Mappings

In chapter 3, it was shown how elements defined in terms of simplex coordinates may be mapped onto elements of arbitrary shape. No suitable mappings were, however, mentioned. This chapter discusses some coordinate transforms that may be used as mappings.

5.1 Simplex Polynomial Interpolation Mappings

In scalar FEM methods, Lagrange interpolation polynomials are often used as basis functions, and as coordinate mappings. Most frequently, they are used to create isoparametric elements (eg. [1, §7.4]), where the same functions are used as basis functions, and as mapping functions.

5.1.1 Mapping Definition

Using the Silvester polynomials to effect Lagrangian interpolation over the simplex element, a coordinate mapping is defined as

$$
\begin{aligned}
x &= \sum x_{ijk}\alpha_{ijk} \\
y &= \sum y_{ijk}\alpha_{ijk},
\end{aligned}
\tag{5.1}
$$

where
$$
\alpha_{ijk} = R_i(n, \lambda_1)R_j(n, \lambda_2)R_k(n, \lambda_3), \qquad i + j + k = n,
\tag{5.2}
$$

n is the polynomial approximation order, and R_i is as defined in [1, §4.2].

This mapping has the effect of mapping the nodes ijk on the reference triangle, to arbitrary nodes, (x_{ijk}, y_{ijk}) in the physical coordinates, while interpolating between them over the rest of the triangle. The position of nodes ijk on the reference triangle is shown in Fig. 5.1.
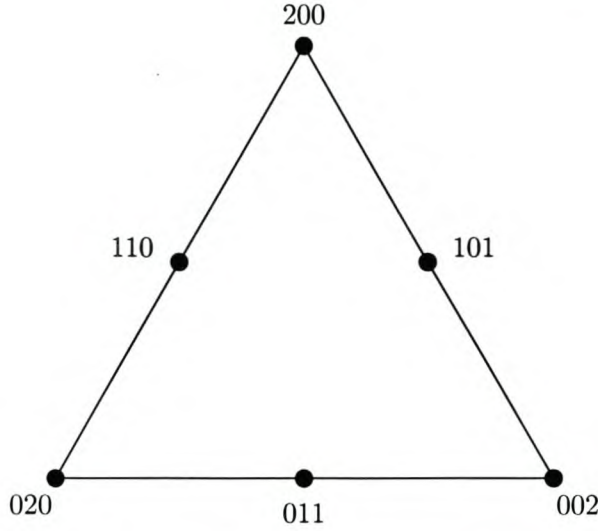
Figure 5.1: Quadratic Simplex Interpolation Reference Triangle

5.1.2 Mapping Compatibility

When mapped elements are used, it is neccesary that they are compatible with other elements used in the same mesh, as described in §4.1.2. In §3.2.4 it is shown that tangential field components defined on the reference triangle, remain tangential when projected onto a mapped element as covariant components. In order to ensure tangential continuity between elements, their tangential unitary vectors must be the same over the whole edge.

Since they use polynomial interpolation, these elements are able to represent a straight line exactly. It can easily be shown that, if the edge interpolation vertices are mapped to equally spaced vertices on the edge of the mapped element, the mapping is identical to that of a linearly mapped triangle on the applicable edge.

In the case of same-order mapping elements bordering, it is enough to ensure the same interpolation points are used for both elements. When differing order elements are bordering, the edge of the higher order element may be made to conform to the edge of the lower order element, by placing its interpolation points on the interpolation curve generated by the lower order element.

5.1.3 Obtaining the Jacobian

Casting these polynomials into functions of only u and v is done by substituting $\lambda_1 = u$, $\lambda_2 = v$, and $\lambda_3 = 1 - u - v$. Obtaining the inverse Jacobian matrix of such a mapping may, for arbitrary mapping order, be simply achieved using simplex differentiation matrices. In the case of lower order

mappings, it is less work to directly differentiate the mapping polynomials by u and v, to yield the Jacobian matrix.

5.2 Parametric Mappings

The interpolatory mappings described in the previous section are not able to fit arbitrary geometries exactly. Mappings exists which allow a mapped element to perfectly fit any curved shape [13], [45], [12].

These papers all describe means of mapping triangles, of which two sides are straight, and one side is described by a parametric curve, onto a straight triangle. Parametric curves are discussed more thoroughly in chapter 6.

The mappings of Zlámal [13] and Mejak [45] are essentially the same, but Zlámal's paper is focused only on the mapping, and hence easier to follow. Villeneuve and Webb's paper [12] defines an alternate mapping, and a re-parameterisation method which reduces basis function distortion. They found their mapping to perform better than Zlámal's.

5.2.1 Mapping Definition

The mapping of Zlámal [13] was implemented. Given a parametrised curve, with

$$\left. \begin{array}{c} x = \phi(s) \\ y = \psi(s) \end{array} \right\}, \qquad 0 \le s \le 1, \tag{5.3}$$

Zlámal's mapping is given by

$$\begin{aligned} x &= x_3 + (x_3 - x_1)u + (x_3 - x_2)v + (1 - u - v)\Phi(v) \\ y &= y_3 + (y_3 - y_1)u + (y_3 - y_2)v + (1 - u - v)\Psi(v), \end{aligned} \tag{5.4}$$

where x_i, y_i are as defined in Fig. 5.2,

$$\begin{aligned} \Phi &= \frac{\phi(v) - x_3 - (x_2 - x_3)v}{1 - v} \\ \Psi &= \frac{\psi(v) - y_3 - (y_2 - y_3)v}{1 - v}, \end{aligned} \tag{5.5}$$

and it it has been assumed that

$$\begin{aligned} (\phi(0), \psi(0)) &= (x_3, y_3) \\ (\phi(1), \psi(1)) &= (x_2, y_2). \end{aligned} \tag{5.6}$$

While (5.5) appears to be singular at $v = 1$, applying L'Hôpital's rule yields

$$\begin{aligned} \lim_{v \to 1^-} \Phi(v) &= (x_2 - x_3) - \phi'(1) \\ \lim_{v \to 1^-} \Psi(v) &= (y_2 - y_3) - \psi'(1). \end{aligned} \tag{5.7}$$
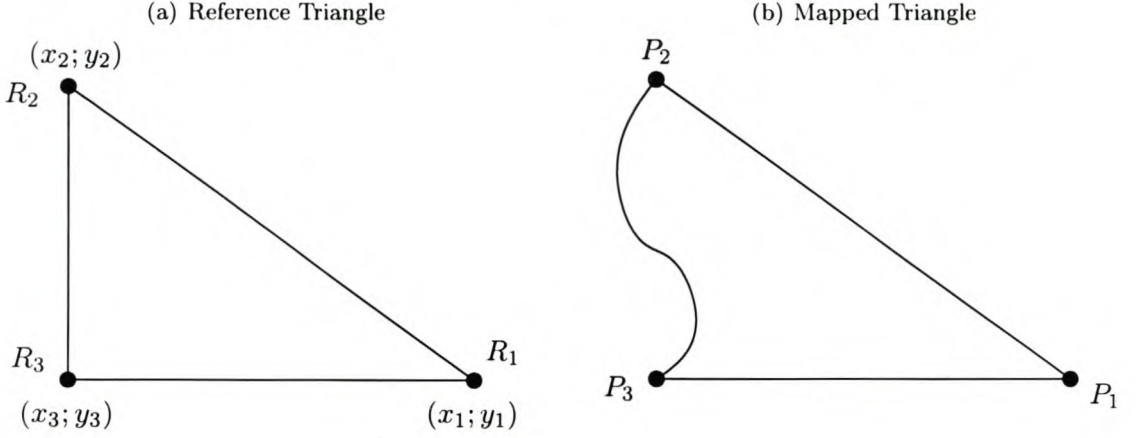
(a) Reference Triangle

(b) Mapped Triangle

Figure 5.2: Zlámal's Mapping

This mapping maps the reference triangle $R_1R_2R_3$ onto the "curved" triangle $P_1P_2P_3$. R_3R_1 and R_1R_2 are respectively mapped to straight lines P_3P_1 and P_1P_2. It can also be seen that, by omitting the mapping terms, $(1-u-v)(\Phi$ or $\Psi)$ from (5.4), it degenerates into a linear triangular mapping.

5.2.2 Obtaining the Jacobian

The mapping given by (5.4) is defined in terms of unknown parametric curve functions. By formal differentiation, a general expression for the Jacobian matrix, in terms of u, v, the parametric curve functions, and their derivatives may be obtained. This general expression may then be utilised for any parametric curve, provided that the curve functions are at least once differentiable.

5.2.3 Mapping Compatibility

The inter-element compatibility constraints, as described in §5.1.2, is now considered. Compatibility with other elements on the straight edges, requires the mapping on those edges to be linear. On edge R_3R_1, (5.5) degenerates to 0, and on edge R_1R_2, $(1 - u - v) = 0$. In both cases the mapping term is zero, and the mapping becomes linear on the edge.

It is possible to ensure conformance when two "curved" triangles share a common curved edge. In this case,

$$\begin{aligned}
(\phi_1(s), \psi_1(s)) &= (\phi_2(s), \psi_2(s)) \qquad \text{or,} \\
(\phi_1(s), \psi_1(s)) &= (\phi_2(1 - s), \psi_2(1 - s))
\end{aligned} \tag{5.8}$$

is required, where the subscripts refer to the respective triangles. The $1 - s$ case applies when the triangles relative edge orderings are opposite.

5.3 Validity of a Mapping

In the previous sections, potential coordinate mappings have been discussed. It was stated in §3.2.2 that a valid mapping must be one to one, and that its Jacobian should be non-vanishing.

The requirement that the Jacobian must be one to one, and non-vanishing, or at least, finite everywhere, is essentially the same. The Jacobian represents the dilation of area, as one set of coordinates is mapped to another. Where the Jacobian vanishes, it means that a finite area of the one domain, is mapped onto one point in the other. This clearly precludes the mapping from being one to one. A similar argument holds when the magnitude of the Jacobian approaches infinity.

With the Jacobian having been obtained, it is still unknown if a given mapping will have a non-vanishing Jacobian, and be one to one. There are no hard and fast rules describing when a polynomial mapping will satisfy these requirements[1, §4.2]. Similarly, Zlámal's mapping is claimed to have a non-zero Jacobian provided that the triangulation is fine enough. No bounds are, however, specified.

One may form a graphical picture of a mapping's validity, and the level of distortion it introduces, by plotting lines of constant coordinate in reference, and mapped, coordinates. The change in area of the grid squares, after having been mapped, represent the magnitude of the Jacobian.

Should any of the mapped squares shrink to a dot, the Jacobian would tend to zero there, and the mapping is probably unusable. Smoothly changing coordinate lines, and roughly constant mapped square area, would indicate a workable mapping.

Fig. 5.3 shows several possible mappings, using the quadratic simplex interpolation as an example. Fig. 5.3b shows an acceptable mapping. It can be seen that the lines of constant coordinate are smooth, and that the magnitude of the Jacobian is finite. Fig. 5.3c shows a mapping that is clearly unacceptable. This mapping was obtained by swapping interpolation nodes 2 and 3 of the previous mapping. Fig. 5.3d shown a mapping with straight sides, but non-uniform interpolation node placement. This should be avoided, since it is clear that the coordinates are highly distorted near node 4, yet no improvement in geometry modelling is to be had.
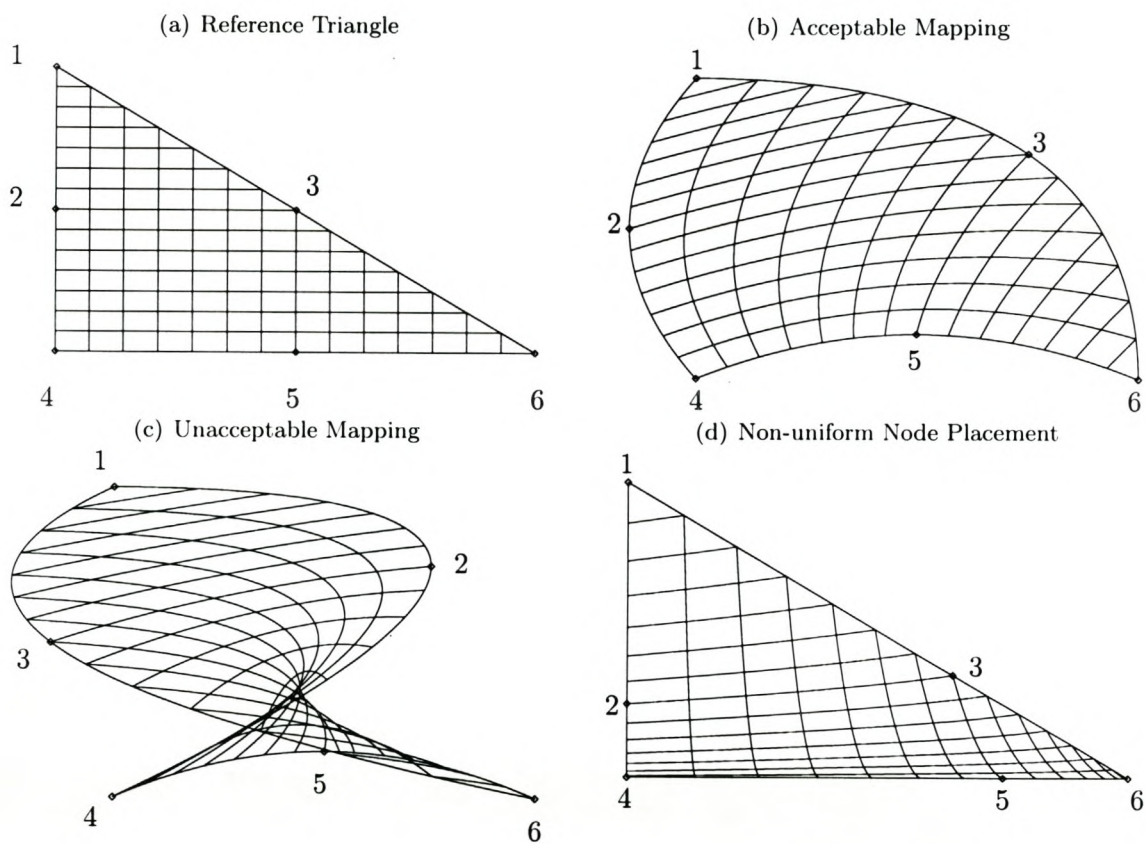
(a) Reference Triangle

(b) Acceptable Mapping

(c) Unacceptable Mapping

(d) Non-uniform Node Placement

Figure 5.3: Quadratic Mappings: the Good, the Bad and the Ugly...

38

Chapter 6

Parametric Curves

In chapter 5, coordinate mappings involving parametric curves were defined. No suitable curves were, however, mentioned. This chapter discusses parametric curves, which are well known in the field of computer graphics.

6.1 General Parametric Curves

Parametric curves are defined in terms of a single parameter, hence their name. A parametric curve in 3D, is expressed in terms of functions of the single parameter, s,

$$\begin{aligned} x &= \phi(s) \\ y &= \psi(s) \\ z &= \chi(s), \end{aligned} \tag{6.1}$$

where ϕ, ψ and χ are arbitrary functions of s. For a 2D curve, the z function is simply omitted. The notation

$$\mathbf{p}(s) = \begin{bmatrix} \phi(s) \\ \psi(s) \\ \chi(s) \end{bmatrix} \tag{6.2}$$

may also be used.

The parameter, s, is often taken to represent a quantity of physical significance, such as time in the case of the curve describing motion in space. In other cases, this parameter is of no importance, such as when parametric curves are used as a well defined way of describing a curve geometry, such as might be used in a CAD system, eg. [46].

In the context of element mapping, it is merely the geometrical description that is of interest. In a particular region of interest, s is usually normalised such that it runs from 0 to 1 along the section of a curve in this region.

6.1.1 Parametric and Geometric Continuity

When multiple parametric curves are joined, various continuity conditions may be imposed where they join. Supposing the two curves join at a point, $\mathbf{p}_j$, the most basic continuity would require that they actually meet at $\mathbf{p}_j$. This is known as C^0 parametric continuity.

Higher orders of parametric continuity is related to the parametric derivatives of the curves at $\mathbf{p}_j$. Defining the parametric derivatives at point $\mathbf{p}_n$ as

$$
\begin{aligned}
\mathbf{p}_n^s &= \frac{d}{ds}\mathbf{p}(s) \\
\mathbf{p}_n^{ss} &= \frac{d^2}{ds^2}\mathbf{p}(s),
\end{aligned}
\tag{6.3}
$$

C^1 continuity would require, in addition to C^0 continuity, that $\mathbf{p}_j^s$ is equal for both curves. Additionally, C^2 continuity requires that $\mathbf{p}_j^{ss}$ be equal for both curves. Higher order C^n continuity is similarly specified.

Parametric continuity is needed when, for instance, the parametric curve is used to describe a smooth motion along a curve. When parametric curves are used only for geometrical modelling, parametric continuity is unnecessarily restrictive.

A less restrictive form of continuity is described by geometric continuity. G^0 continuity requires that the two curves meet at $\mathbf{p}_j$, and is essentially the same as C^0 continuity. G^1 continuity indicates that the two curves should, additionally, have a common tangent at $\mathbf{p}_j$. G^2 continuity furthermore requires that, the two curves have a common radius of curvature at this point.

6.2 Polynomial Parametric Curves

Polynomial Parametric Curves (PPC) are defined in terms of polynomials of a single parameter. In 2D, a PPC is defined as,

$$
\begin{aligned}
x &= P_x(s) \\
y &= P_y(s),
\end{aligned}
\tag{6.4}
$$

where P_x and P_y are polynomials in s. When dealing with fixed order polynomial curves, they may, in the case of cubic polynomials, be written as

$$
\begin{aligned}
x(s) &= a_x s^3 + b_x s^2 + c_x s + d_x \\
y(s) &= a_y s^3 + b_y s^2 + c_y s + d_y.
\end{aligned}
\tag{6.5}
$$

Equation (6.5) may be written more compactly in matrix form

$$
\mathbf{p}(s) = \mathbf{UA},
\tag{6.6}
$$

where $\mathbf{U} = [s^3 \; s^2 \; s \; 1]$, $\mathbf{A} = [\mathbf{a} \; \mathbf{b} \; \mathbf{c} \; \mathbf{d}]^T$. The entries of $\mathbf{A}$ completely define a PPC.

While the entries in $\mathbf{A}$ completely specify the PPC, it is quite inconvenient to use the algebraic coefficients to specify a curve. Other polynomial bases, which allow the properties of a curve to be more conveniently expressed may be used. The functions used are often referred to as blending functions, as they describe the way different control points are blended together.

6.2.1 Hermite Interpolatory Curves

Using Hermite polynomials as the blending functions, it is possible to directly control the position, as well as the parametric derivatives, and hence, tangent, of the curve at its endpoints.

A Hermite curve may be written in terms of (6.6) as

$$\mathbf{p}(s) = \mathbf{UMB}, \tag{6.7}$$

where $\mathbf{B} = [\mathbf{p}_0 \; \mathbf{p}_1 \; \mathbf{p}_0^s \; \mathbf{p}_1^s]^T$, and $\mathbf{M}$ transforms the coefficients of the Hermite functions into algebraic form. While obtaining $\mathbf{M}$ is fairly easy, it may be found in computer graphics texts, such as [47].

It should be noted that using the tangents at $\mathbf{p}_0$ and $\mathbf{p}_1$ to specify the parametric derivatives $\mathbf{p}_0^s$ and $\mathbf{p}_1^s$, does not completely specify the curve. The magnitudes of the respective derivatives are additional degrees of freedom.

Furthermore, the cubic Hermite curve has the property that $\mathbf{p}(0.5) = (\mathbf{p}_0 + \mathbf{p}_1)/2 + (\mathbf{p}_0^s - \mathbf{p}_1^s)/8$.

6.2.2 Bézier Curves

Bézier curves were invented by Piere Bézier at Renault, for use in CAD modelling. A Bézier curve of degree n is defined in terms of $n + 1$ control points, $\mathbf{p}_0, \mathbf{p}_1, \ldots, \mathbf{p}_n$, and the Bernstein polynomials

$$\mathscr{B}_{k,n}(s) = C(n,k)s^k(1-s)^{n-k}, \tag{6.8}$$

where $C(n,k)$ are the binomial coefficients,

$$C(n,k) = \frac{n!}{k!(n-k)!}. \tag{6.9}$$

In matrix notation, Bézier curves are given as

$$\mathbf{p}(s) = \mathbf{BP}, \tag{6.10}$$

where $\mathbf{B} = [\mathscr{B}_{0,n} \; \mathscr{B}_{1,n} \ldots \mathscr{B}_{n,n}]$, and $\mathbf{P} = [\mathbf{p}_0 \; \mathbf{p}_1 \; \ldots \; \mathbf{p}_n]^T$. It may be written in terms of (6.6), by finding a suitable transform matrix $\mathbf{M}$, such that

$$\mathbf{p}(s) = \mathbf{UMP}. \tag{6.11}$$

Once again, obtaining $\mathbf{M}$ is not difficult, but is listed for various orders of Bézier function in [47]. The points $\mathbf{p}_0, \mathbf{p}_1, \ldots, \mathbf{p}_n$ define the *control polygon* of the Bézier curve. The control polygon for a quadratic Bézier curve is shown in Fig. 6.1.
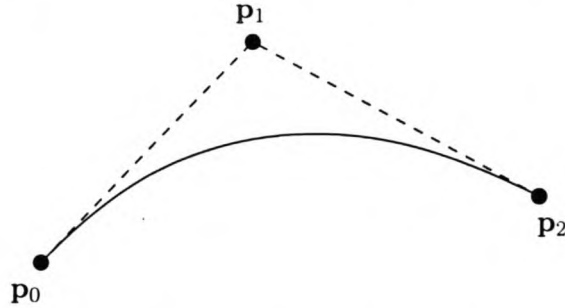

Figure 6.1: Quadratic Bézier Control Polygon

Bézier curves have some useful properties, which make them well suited to CAD work. Some of them are

1. Bézier curves always interpolate their first($\mathbf{p}_0$), and last($\mathbf{p}_n$), control points, when s is respectively zero, and one;

2. parametric derivatives at $\mathbf{p}_0$ and $\mathbf{p}_n$ are respectively given by $\mathbf{p}_1 - \mathbf{p}_0$ and $\mathbf{p}_n - \mathbf{p}_{n-1}$;

3. the rth parametric derivative at the endpoints, are defined by the r control points neighbouring the endpoints.

These properties allow a designer much freedom in specifying the shape of a curve, while also allowing C^1 continuity to be specified graphically.

6.2.3 Interpolatory Spline Curves

The word spline originally referred to a flexible strip draftsmen use to smoothly interpolate a set of points on a drawing. A spline curve is, in general, a curve that can smoothly interpolate an arbitrary number of points in sequence.

Splines are usually defined as a number of piecewise polynomial parametric curves, that meet certain continuity conditions at the points where they meet. One of the first spline curves to be developed was the natural cubic spline, which enforced C^2 continuity at each interpolation point. This is a mathematical representation of the original drafting spline. Many types of splines have been derived, that may be used to satisfy various continuity conditions, and may be found in computer graphics texts, such as [20].

Spline curves are useful when a relatively long curve needs to be interpolated. They provide more accuracy than a single parametric curve of the

same order would have, without requiring the complexity of a higher order curve representation. For this reason, they are often used in CAD systems to represent large structures.

6.2.4 PPC Approximation of Conic Sections

An approximation of conic sections, in terms of the Hermite cubic parametric curve as defined in §6.2.1, is given by [47]. Three control points, $\mathbf{p}_0$, $\mathbf{p}_1$ and $\mathbf{p}_2$, as defined in Fig. 6.2 are used.
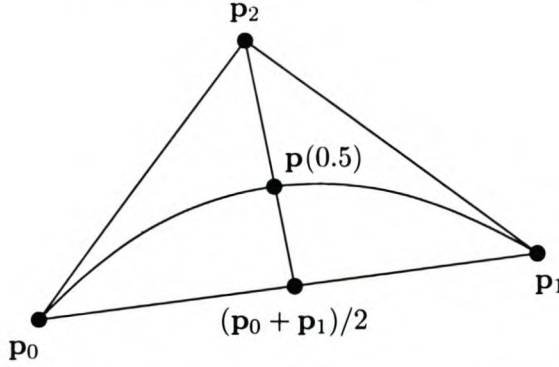

Figure 6.2: Cubic Hermite Parametric Conic Approximation

The tangent of the curve at the end points $\mathbf{p}_0$, $\mathbf{p}_1$, are respectively proportional to $\mathbf{p}_2 - \mathbf{p}_0$ and $\mathbf{p}_1 - \mathbf{p}_2$. As noted in §6.2.1, the specification of the tangents at the endpoints still leave two degrees of freedom.

Using $\mathbf{B}$ as defined in §6.2.1, and the property $\mathbf{p}(0.5) = (\mathbf{p}_0 + \mathbf{p}_1)/2 + (\mathbf{p}_0^s - \mathbf{p}_1^s)/8$, we write

$$\mathbf{B} = [\mathbf{p}_0 \ \mathbf{p}_1 \ q(\mathbf{p}_2 - \mathbf{p}_0) \ q(\mathbf{p}_1 - \mathbf{p}_2)]. \tag{6.12}$$

The value of q is then chosen such that the approximate curve interpolates the real curve at $\mathbf{p}(0.5)$.

For parabolas, this curve is exact. For a circle arc sub-tending less than $45°$, [47] claims $\Delta R/R < 5 \times 10^{-6}$, where ΔR is the error in radius. In general, the approximation error should be of order $O(h^{p+1})$, where p is the order of the approximation, and h the distance between interpolation points[41].

6.3 Rational Parametric Curves

Rational parametric curves may be defined as the ratio of two PPC functions. Quadratic rational splines have the desirable property that they are able

to exactly represent any conic section. They may be written in terms of quadratic Bézier curves

$$\mathbf{p}(s) = \frac{w_0 \mathbf{p}_0 \mathscr{B}_{0,2}(s) + w_1 \mathbf{p}_1 \mathscr{B}_{1,2}(s) + w_2 \mathbf{p}_2 \mathscr{B}_{2,2}(s)}{w_0 \mathscr{B}_{0,2}(s) + w_1 \mathscr{B}_{1,2}(s) + w_2 \mathscr{B}_{2,2}(s)}. \tag{6.13}$$

While the weights, w_n, seem to represent three additional degrees of freedom, any quadratic rational curve may be written as [48]

$$\mathbf{p}(s) = \frac{\mathbf{p}_0 \mathscr{B}_{0,2}(s) + w_1 \mathbf{p}_1 \mathscr{B}_{1,2}(s) + \mathbf{p}_2 \mathscr{B}_{2,2}(s)}{\mathscr{B}_{0,2}(s) + w_1 \mathscr{B}_{1,2}(s) + \mathscr{B}_{2,2}(s)}. \tag{6.14}$$

The control points define the start and end points, as well as the tangent of the curve at the end points in the same way as a normal Bézier curve. The weight, w_1, pulls the curve towards $\mathbf{p}_1$. Setting $w_1 = 1$ recovers the quadratic Bézier curve, since the sum of the Bernstein functions is one.

In order to exactly represent a conic section, the control polygon needs to be set up, which is quite straight forward, and a suitable weight, w_1 must be found. This may be done, by noting that the curvatures κ_0 and κ_1 at $\mathbf{p}_0$ and $\mathbf{p}_2$ is given by[48]

$$\begin{aligned}
\kappa_0 &= \frac{w_0 w_2}{w_1^2} \frac{A}{l_0^3} \\
\kappa_1 &= \frac{w_0 w_2}{w_1^2} \frac{A}{l_1^3},
\end{aligned} \tag{6.15}$$

where A is the area of the triangle formed by the control polygon, and l_0 and l_1 represent the length of, respectively, the first and second control polygon leg.

6.4   Application to 3D

Parametric curve concepts may also be generalised to higher dimensional objects, such as surfaces, and volumes. Parametric surfaces, also called patches, may be defined as the function of two parameters. They are usually defined as polynomial tensor products of the curves described above.

A Bézier patch, for instance, is defined as

$$\mathbf{p}(s,t) = \sum_{i=0}^{m} \sum_{j=0}^{n} \mathbf{p}_{ij} \mathscr{B}_{i,m}(s) \mathscr{B}_{j,n}(t). \tag{6.16}$$

$\mathscr{B}_{i,m}, \mathscr{B}_{j,n}$ are the Bernstein polynomials, as before, and the points $\mathbf{p}_{ij}$ form a $(m+1) \times (n+1)$ rectangular array of control points. These control points make up the vertices of the characteristic Bézier polyhedron. A rational surface may, similarly, be defined as

$$\mathbf{p}(s,t) = \frac{\sum_{i=0}^{m} \sum_{j=0}^{n} \mathbf{p}_{ij} w_{ij} \mathscr{B}_{i,m}(s) \mathscr{B}_{j,n}(t)}{\sum_{i=0}^{m} \sum_{j=0}^{n} w_{ij} \mathscr{B}_{i,m}(s) \mathscr{B}_{j,n}(t)}. \tag{6.17}$$

These patches only describe one surface, as the function of two parameters. If the tetrahedral equivalent to Zlámal's mapping could be found, one might mesh a domain in such a way that only one triangle on each tetrahedron is curved, and use these patches to define a surface on the curved tetrahedron.

Another approach would be to use hyper-patches. Analogous to the surface patches described above, they may be used to represent "volumes" in 4D hyper-space. Ignoring the fourth dimension, they may be used to describe volumes in 3D space. Such a Bézier form is, in fact, suggested in [14]. Similarly, the 3D surface patches previously described may be applied to 2D problems.

Chapter 7

Results

This chapter presents the results obtained using the code previously outlined. The code was applied to four waveguide geometries that have known analytical solutions. These are, the rectangular, circular, and elliptic waveguides, and the higher order modes of a circular coaxial structure.

7.1 Waveguide Geometries and Solutions

This section discusses the analytical solutions of the waveguides under consideration in this chapter. These results are the basis of comparison used to evaluate the efficiency of the implemented FEM code.

All the waveguides considered here support modes which are, either pure TE waves, or pure TM modes. A TE mode may be completely characterised by its $\hat{z}$ directed $\vec{H}$ field, and its $\hat{z}$ directed cutoff wave number. The same applies for the $\hat{z}$ directed $\vec{E}$ field of a TM mode.

7.1.1 TE and TM Modes

TE waves are characterised by $E_z = 0$, and $H_z \neq 0$. The TE modes of a constant cross-section waveguide may be obtained[18] by assuming an H_z z dependence of $e^{-j\beta z}$, hence

$$H_z(x, y, z) = h_z(x, y)e^{-j\beta z}, \tag{7.1}$$

where $\beta = \sqrt{k^2 - k_c^3}$, and k_c is the cutoff wave number. Now the 3D Helmholtz equation is reduced to

$$\left(\frac{\delta^2}{\delta x^2} + \frac{\delta^2}{\delta y^2} + k_c^2 \right) h_z = 0. \tag{7.2}$$

Now (7.2) may be solved subject to the boundary conditions of the specific guide geometry. Once H_z has been solved, the other field components

46

may be found:

$$H_x = \frac{-j\beta}{k_c^2} \frac{\delta H_z}{\delta x},$$
$$H_y = \frac{-j\beta}{k_c^2} \frac{\delta H_z}{\delta y},$$
$$E_x = \frac{-j\omega\mu}{k_c^2} \frac{\delta H_z}{\delta y},$$
$$E_y = \frac{j\omega\mu}{k_c^2} \frac{\delta H_z}{\delta x}.$$

(7.3)

TM waves are characterised by $H_z = 0$ and $E_z \neq 0$. Assuming again a z dependence, this time for E_z, of $e^{-j\beta z}$,

$$E_z(x, y, z) = e_z(x, y)e^{-j\beta z}.$$

(7.4)

As before, $\beta = \sqrt{k^2 - k_c^2}$. The 3D Helmholtz equation is now reduced to

$$\left(\frac{\delta^2}{\delta x^2} + \frac{\delta^2}{\delta y^2} + k_c^2\right) e_z = 0.$$

(7.5)

Once E_z has been solved, the other field components may be found:

$$H_x = \frac{j\omega\epsilon}{k_c^2} \frac{\delta E_z}{\delta y},$$
$$H_y = \frac{-j\omega\epsilon}{k_c^2} \frac{\delta E_z}{\delta x},$$
$$E_x = \frac{-j\beta}{k_c^2} \frac{\delta E_z}{\delta x},$$
$$E_y = \frac{-j\beta}{k_c^2} \frac{\delta E_z}{\delta y}.$$

(7.6)

Throughout this section, the convention

$$E_x(x, y, z) = e_x(x, y)e^{-j\beta z},$$
$$E_y(x, y, z) = e_y(x, y)e^{-j\beta z},$$
$$E_z(x, y, z) = e_z(x, y)e^{-j\beta z},$$

(7.7)

is used.

7.1.2 Rectangular Waveguide

A rectangular waveguide geometry, with breadth a, and height b is shown in Fig. 7.1. The waveguide is assumed to be homogeneously filled with a material of permitivity ϵ and permiability μ. The waveguide walls are assumed to be perfect conductors.
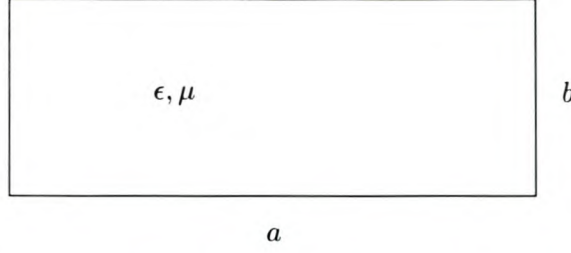
Figure 7.1: Rectangular Waveguide Geometry

For TE and TM modes, (7.2) and (7.5) are, respectively, to be solved. They may be solved by the method of separation of variables in Cartesian coordinates.

The boundary conditions for TE modes are

$$
\begin{aligned}
e_x(x, y) &= 0, && \text{at } y = 0, b, \\
e_y(x, y) &= 0, && \text{at } x = 0, a.
\end{aligned}
\tag{7.8}
$$

The solution of H_z, for the TE_{mn} mode, is found as

$$
H_z(x, y, z) = A_{mn} \cos\left(\frac{m\pi x}{a}\right) \cos\left(\frac{n\pi y}{b}\right) e^{-j\beta z},
\tag{7.9}
$$

where $\beta = \sqrt{k^2 - k_{c_{mn}}^2}$, and

$$
k_{c_{mn}} = \sqrt{\left(\frac{m\pi}{a}\right)^2 + \left(\frac{n\pi}{b}\right)^2},
\tag{7.10}
$$

and A_{mn} is an arbitrary magnitude constant. When $k > k_{c_{mn}}$, β is real, and the TE_{mn} mode propagates.

Using (7.3), the transverse E field components may be found as

$$
\begin{aligned}
E_x &= \frac{j\omega\mu n\pi}{k_c^2 b} A_{mn} \cos\left(\frac{m\pi x}{a}\right) \sin\left(\frac{n\pi y}{b}\right), \\
E_y &= \frac{-j\omega\mu m\pi}{k_c^2 a} A_{mn} \sin\left(\frac{m\pi x}{a}\right) \cos\left(\frac{n\pi y}{b}\right).
\end{aligned}
\tag{7.11}
$$

From these transverse E field expressions, and the boundary conditions (7.8), the cutoff wave number (7.10), and assuming $a > b$, it can be seen that the non-vanishing TE mode, with the lowest cutoff frequency, is the TE_{10} mode. The cutoff frequency of this modes, corresponds to $a = \lambda/2$ in the wave-guide medium.

The boundary conditions for the TM modes are

$$
\begin{aligned}
e_z(x, y) &= 0, && \text{at } y = 0, b, \\
e_z(x, y) &= 0, && \text{at } x = 0, a.
\end{aligned}
\tag{7.12}
$$

The solution of E_z for the TM_{mn} mode, is found as

$$E_z(x, y, z) = B_{mn} \sin\left(\frac{m\pi x}{a}\right) \sin\left(\frac{n\pi y}{b}\right) e^{-j\beta z}, \qquad (7.13)$$

where β and $k_{c_{mn}}$ is as for the TE modes.

From the boundary conditions (7.12), the cutoff wave number (7.10), and the assumption $a > b$, it can be seen that the non-vanishing TM mode, with the lowest cutoff frequency, is the TM_{11} mode. Since this mode has a higher cutoff frequency than the TE_{10} mode, the TE_{10} mode is the dominant mode of the waveguide.

7.1.3   Circular Waveguide

A circular waveguide geometry, with radius a is shown in Fig. 7.2. The waveguide is assumed to be homogeneously filled with a material of permitivity ϵ and permiability μ. The waveguide walls are assumed to be perfect conductors.
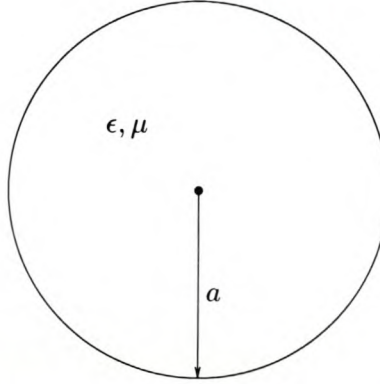

Figure 7.2: Circular Waveguide Geometry

Writing (7.2) and (7.5) in cylindrical coordinates, it is possible to solve them using the method of separation of variables. From the solution of the respective equations, the TE and TM modes may be found.

The equivalent of (7.3) and (7.6) in cylindrical coordinates are

$$E_\rho = \frac{-j}{k_c^2}\left(\beta\frac{\delta E_z}{\delta\rho} + \frac{\omega\mu}{\rho}\frac{\delta H_z}{\delta\phi}\right),$$

$$E_\phi = \frac{-j}{k_c^2}\left(\frac{\beta}{\rho}\frac{\delta E_z}{\delta\phi} - \omega\mu\frac{\delta H_z}{\delta\rho}\right),$$

$$H_\rho = \frac{j}{k_c^2}\left(\frac{\omega\epsilon}{\rho}\frac{\delta E_z}{\delta\phi} - \beta\frac{\delta H_z}{\delta\rho}\right), \qquad (7.14)$$

$$H_\phi = \frac{-j}{k_c^2}\left(\omega\epsilon\frac{\delta E_z}{\delta\rho} + \frac{\beta}{\rho}\frac{\delta H_z}{\delta\phi}\right),$$

where, as before, $\beta = \sqrt{k^2 - k_c^2}$.

For TE modes, the boundary condition is

$$E_\phi(\rho, \phi, z) = 0, \qquad \text{at } \rho = a. \qquad (7.15)$$

The solution of H_z for the TE$_{nm}$ modes, is found as

$$H_z(\rho, \phi, z) = (A_{nm} \sin(n\phi) + B_{nm} \cos(n\phi)) J_n(k_{c_{nm}} \rho) e^{-j\beta z}, \qquad (7.16)$$

where J_n are Bessel functions of the first kind, A_{nm} and B_{nm} are arbitrary magnitude constants, and $k_{c_{nm}}$ the cutoff wavenumber for the TE$_{nm}$ mode.

Using (7.14) to find

$$E_\phi = \frac{j\omega\mu}{k_c}(A_{nm} \sin(n\phi) + B_{nm} cos(n\phi)) J_n'(k_c \rho), \qquad (7.17)$$

the boundary condition (7.15) may be satisfied by setting

$$J_n'(k_{c_{nm}} a) = 0. \qquad (7.18)$$

Defining the roots of $J_n'(x)$ as p_{nm}', so that $J_n'(p_{nm}') = 0$, where p_{nm}' is the mth root of J_n', the cutoff wavenumber may be found as

$$k_{c_{nm}} = \frac{p_{nm}'}{a}. \qquad (7.19)$$

Values of p_{nm}' are given in mathematical tables, or may be numerically determined using a suitable software package.

From the form of the solutions, it can be seen that n refers to the number of circumferential (ϕ) field variations, and m refers to the number of radial (ρ) field variations. Since $m \geq 1$, there is no TE$_{10}$ mode.

For TM modes, the boundary condition is

$$E_z(\rho, \phi, z) = 0, \qquad \text{at } \rho = a. \qquad (7.20)$$

The solution of E_z for the TM$_{nm}$ modes, is the same as H_z for the TE modes,

$$E_z(\rho, \phi, z) = (A_{nm} sin(n\phi) + B_{nm} \cos(n\phi)) J_n(k_{c_{nm}} \rho) e^{-j\beta z}. \qquad (7.21)$$

The boundary condition, (7.20) may be satisfied by setting

$$J_n(k_{c_{nm}} a) = 0. \qquad (7.22)$$

Defining the roots of $J_n(x)$ as p_{nm}, so that $J_n(p_{nm}) = 0$, where p_{nm} is the mth root of J_n, the cutoff wavenumber may be found as

$$k_{c_{nm}} = \frac{p_{nm}}{a}. \qquad (7.23)$$

The mode with the lowest frequency cutoff wave-number, is the TE$_{11}$ mode. This is due to the properties of Bessel functions.

The ratio of A_{nm} to B_{nm} is arbitrary. By rotating the waveguide, it is always possible to set either A_{nm} or B_{nm} to zero.

7.1.4 Elliptic Waveguide

An elliptic waveguide geometry, with semi-major axis a, semi-minor axis b, and focal distance $2q$ is shown in Fig. 7.3. The waveguide is assumed to be homogeneously filled with a material of permitivity ϵ and permiability μ. The waveguide walls are assumed to be perfect conductors.
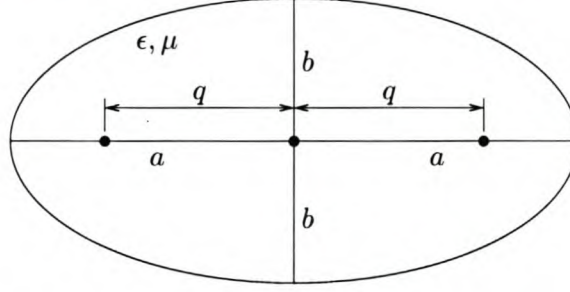

Figure 7.3: Elliptic Waveguide Geometry

It is possible to solve (7.2) and (7.5), by writing them in an elliptic coordinate system. An elliptic coordinate system may be defined by the transform

$$x = q \cosh \xi \cos \eta$$
$$y = q \sinh \xi \sin \eta, \tag{7.24}$$

where $2q$ is the focal distance. The ξ coordinate represents con-focal ellipses, and the η coordinate represents con focal hyperbolas. If the bounding ellipse is given by $\xi = \xi_0$, the eccentricity of the boundary is $e = \cosh^{-1} 1/\xi_0$.

Elliptic cylindrical waves may be expanded in terms of the Mathieu functions[39]. Mathieu functions are solutions of the differential equation[49]

$$\frac{d^2 y}{dv^2} + (r - 2\chi \cos 2v)y = 0. \tag{7.25}$$

Modified Mathieu functions are given by the solutions to

$$\frac{d^2 f}{du^2} - (r - 2\chi \cosh 2u)f = 0. \tag{7.26}$$

Solutions of (7.26) may be obtained by substituting $u = jv$ into solutions of (7.25).

Solutions to (7.25) are periodic with periodicity π or 2π, for certain specific values of r, called characteristic values. Periodic solutions are required for the angular dependence, i.o.w. in the η coordinate. The values of r depends on q, and whether the solution is even, or odd.

Mathieu functions can have odd, or even symmetry. The, respectively even and odd, Mathieu functions are written as $ce_m(r_m, \chi, \xi)$ and $ce_s(r_m, \chi, \xi)$.

The respective modified Mathieu functions are written as $Ce_m(r_m, \chi, \eta)$ and $Ce_s(r_m, \chi, \eta)$. Note that r_m differs between the even and odd functions. The subscript m refers to the function of the mth characteristic value. The r_m will hence be dropped form the functional notation. A function of r_m will be referred to as a Mathieu function of order m.

For TE modes, the boundary conditions are

$$E_\eta(\xi, \eta, z) = 0 \qquad \text{at } \xi = \xi_0. \tag{7.27}$$

Even $_eTE_{mn}$ mode solutions may be found as[19]

$$E_z =_e A_{mn} Ce_c(e\chi_{mn}, \xi) ce_c(e\chi_{mn}, \eta) e^{-j\beta z}, \tag{7.28}$$

where $_eA_{mn}$ is an arbitrary magnitude constant, and β is as before. The odd $_oTE_{mn}$ mode solutions are the same, except for the substitution of the odd Mathieu functions.

From E_z, the solution of E_η may be found as

$$E_\eta = \frac{_eA_{mn} Ce_m'(e\chi_{mn}', \xi) ce_m(e\chi_{mn}', \eta)}{-jkq\sqrt{\cosh^2 \xi - \cos^2 \eta}}. \tag{7.29}$$

From 7.29, the boundary condition (7.27) may be satisfied for a waveguide of given eccentricity by setting[50]

$$Ce_c'(e\chi_{mn}', \xi_0) = 0, \tag{7.30}$$

where $_e\chi_{mn}'$ refers to the nth root of the derivative of the mth order even Mathieu function.

For TM modes, the boundary condition is

$$E_z(\xi, \eta, z) = 0 \qquad \text{at } \xi = \xi_0. \tag{7.31}$$

Even $_eTM_{mn}$ mode solutions may be found as

$$E_z =_e B_{mn} Ce_c(e\chi_{mn}, \xi) ce_c(e\chi_{mn}, \eta) e^{-j\beta z}, \tag{7.32}$$

where $_eB_{mn}$ is an arbitrary magnitude constant, and β is as before. The odd $_oTM_{mn}$ mode solutions are the same, except for the substitution of the odd Mathieu functions.

The boundary condition (7.31) may be satisfied for a waveguide of given eccentricity by setting

$$Ce_c(e\chi_{mn}, \xi_0) = 0, \tag{7.33}$$

where $_e\chi_{mn}$ refers to the nth root of the mth order even Mathieu function.

The cut-off wavenumbers may be found in terms of the various χ roots. On omission of the mode designations[19],

$$k_{ci} = \frac{\chi i}{q}. \tag{7.34}$$

An efficient evaluation method for Mathieu functions is presented in [51]. The only general purpose mathematical package that supports the evaluation of Mathieu functions, is Mathematica[52].

7.1.5 Circular Coaxial Waveguide

A circular, coaxial waveguide geometry with inner radius a, and outer radius b is shown in Fig. 7.4. The waveguide is assumed to be homogeneously filled with a material of permitivity ϵ and permiability μ. The waveguide walls are assumed to be perfect conductors. Coaxial waveguides have a dominant
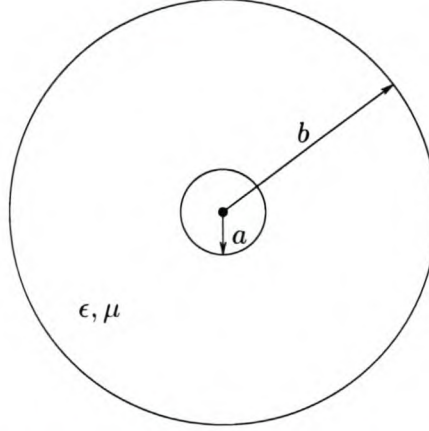

Figure 7.4: Coaxial Circular Waveguide Geometry

Transverse Electro-Magnetic (TEM) mode, with zero cutoff frequency. This mode is the one typically used for applications. The TEM mode is easily determined, since TEM modes have the same field distribution as the static field of a given structure.

The TEM modes are easy to determine analytically, and is in any case not solved by the high-frequency formulation used here. Higher-order TE and TM modes are, however, also supported by a coaxial structure. It is of practical interest to know what the cutoff frequency of the lowest-order TE or TM mode is, since this typically sets the operational frequency limits of a coaxial structure.

As for the circular waveguide, (7.2) and (7.5) may be solved by writing them in cylindrical coordinates. From the solution of the respective equations, the TE and TM modes may be found.

For TE modes, the boundary conditions are

$$E_\phi(\rho, \phi, z) = 0, \qquad \text{at } \rho = a, b. \tag{7.35}$$

The solution of H_z for the TE$_{nm}$ modes, is found as

$$H_z(\rho, \phi, z) = (A_{nm} \sin(n\phi) + B_{nm} \cos(n\phi))(C_{nm} J_n(k_{c_{nm}}\rho) + D_{nm} Y_n(k_{c_{nm}}\rho)), \tag{7.36}$$

where J_n and Y_n are respectively, Bessel functions of the first and second kind, A_{nm}, B_{nm}, C_{nm}, and D_{nm} are arbitrary magnitude constants, and $k_{c_{nm}}$ the cutoff wavenumber for the TE$_{nm}$ mode.

Using (7.14) to find

$$E_\phi = \frac{j\omega\mu}{k_c}(A_{nm}\sin(n\phi) + B_{nm}cos(n\phi))(C_{nm}J_n^{'}(k_c\rho) + D_{nm}Y_n(k_{c_{nm}}\rho)e^{-j\beta z},$$
(7.37)

the boundary condition (7.35) may be satisfied by setting

$$\begin{aligned} C_{nm}J_n^{'}(k_{c_{nm}}a) + D_{nm}Y_n^{'}(k_{cnm}a) = 0, \\ C_{nm}J_n^{'}(k_{c_{nm}}b) + D_{nm}Y_n^{'}(k_{cnm}b) = 0. \end{aligned}$$
(7.38)

Since this is a homogeneous set of equations, the only nontrivial ($C \neq 0, D \neq 0$) solution occurs when the determinant is zero. Thus,

$$J_n^{'}(k_{c_{nm}}a)Y_n^{'}(k_{c_{nm}}b) = J_n^{'}(k_{c_{nm}}b)Y_n^{'}(k_{c_{nm}}a).$$
(7.39)

Since (7.35) is a transcendental equation, it has to be solved numerically.

The solution of the TM modes is identical, excepting the boundary conditions. For TM modes, the boundary conditions are

$$E_z(\rho, \phi, z) = 0, \qquad \text{at } \rho = a, b.$$
(7.40)

The solution of E_z for the TM$_{nm}$ modes, is found as

$$E_z(\rho, \phi, z) = (A_{nm}\sin(n\phi) + B_{nm}\cos(n\phi))(C_{nm}J_n(k_{c_{nm}}\rho) + D_{nm}Y_n(k_{c_{nm}}\rho)).$$
(7.41)

The boundary condition (7.40) may be satisfied by setting

$$\begin{aligned} C_{nm}J_n(k_{c_{nm}}a) + D_{nm}Y_n(k_{cnm}a) = 0, \\ C_{nm}J_n(k_{c_{nm}}b) + D_{nm}Y_n(k_{cnm}b) = 0. \end{aligned}$$
(7.42)

Similar to the TE case, this yields the transcendental equation

$$J_n(k_{c_{nm}}a)Y_n(k_{c_{nm}}b) = J_n(k_{c_{nm}}b)Y_n(k_{c_{nm}}a).$$
(7.43)

As for the circular waveguide, the ratio of A_{nm} to B_{nm} is arbitrary. Similarly, the waveguide may be rotated to set either to zero.

7.2 Performance of Unmapped Elements

The performance of unmapped (straight) elements are investigated in this section. In order to establish the best possible performance of a given base, a geometry with straight sides is solved. In order to provide a base of comparison for mapped elements, a curved geometry is also investigated. The basis name contractions used throughout, are shown in table 7.1.

Contraction	Tangential Order	Normal Order
CT/LN	Constant	Linear
LT/LN	Linear	Linear
LT/QN	Linear	Quadratic
QT/QN	Quadratic	Quadratic
QT/CuN	Quadratic	Cubic
CuT/CuN	Cubic	Cubic
CuT/Q4N	Cubic	Quadric
Q4N/Q4N	Quadric	Quadric
Q4T/Q5N	Quadric	Quintic
Q5N/Q5N	Quintic	Quintic

Table 7.1: Basis Name Contractions

	1	2	3	4	5	6	7	8	9	10	11	12
TE k_c^2/π^2	1	4	4	5	8	9	13	16	16	17	20	20
TM k_c^2/π^2	5	8	13	17	20	20	25	29	32	37	40	40

Table 7.2: First 12 cutoff wave numbers k_c of a rectangular waveguide, with breadth $a = 1$ m and height $b = 0.5$ m.

7.2.1 Domains with Straight Boundaries

A rectangular waveguide geometry, as described in §7.1.2 is investigated. The results are for a waveguide with a breadth $a = 1$ m, and a height $b = 0.5$ m. The first 12 cutoff wavenumbers of the TE and TM modes for this waveguide is given in table 7.2

The RMS error over these 12 modes are shown in Fig. 7.5. From the gradients of each basis' error, it can be seen that the convergence is faster, as higher order basis functions are used. Use of a higher order base results in better solution efficiency w.r.t. DOFs in almost all cases.

(a) RMS Error over 12 TE modes   (b) RMS Error over 12 TM modes
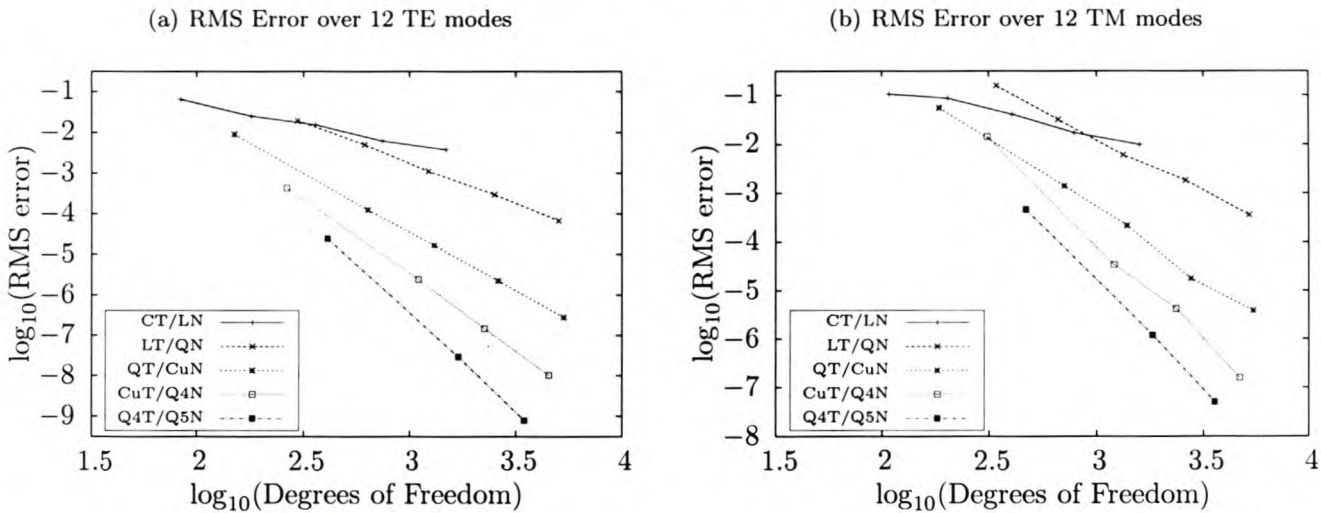

Figure 7.5: Performance of Unmapped Elements: Rectangular Waveguide

The trends for the TE and TM modes are very similar. The TE solutions have smaller errors than the TM, and the TM LT/QN solution is not uniformly superior to CT/LN, as it was for the TE modes. The larger TM mode errors may be ascribed to the natural, rather than enforced, boundary conditions, and the fact that the TM modes correspond to somewhat higher frequencies.

7.2.2 Mixed vs. Full-order Elements

In §4.3.2, it was shown that mixed order elements have the same asymptotic behaviour as full-order elements. In some cases, it might still be beneficial to use full-order elements.

For the rectangular waveguide, the curl, and the field itself, should be of similar importance. To confirm this, mixed-order bases are compared to full-order bases. Fig. 7.6 shows the comparative results.

In general, the full- and mixed-order bases converge at the same rate. The full-order bases are, however, less efficient than the mixed-order bases.
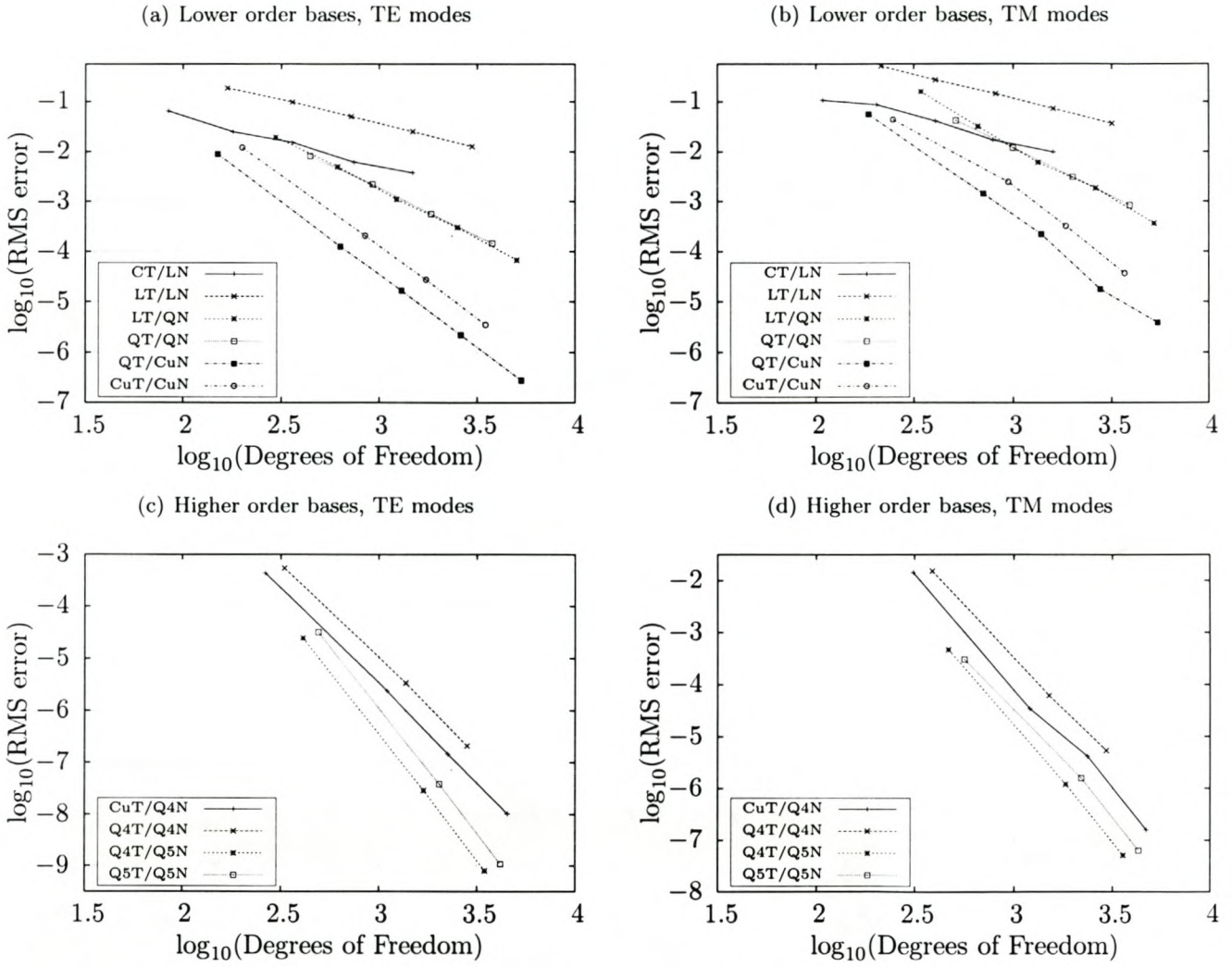
Figure 7.6: Comparison of Full- and Mixed Order Elements: Rectangular Waveguide

Somewhat surprisingly, the full-order bases also show a larger error when exactly the same discretisation is used. The exception to the general rule, is the LT/QN and QT/QN pair, which perform most similarly.

7.2.3 Domains with Curved Boundaries

In order to test the efficiency of unmapped elements in curved domains, they were applied to the circular waveguide geometry described in §7.1.3. The results are for a waveguide with a radius of 1 m. The first 12 cutoff wavenumbers of the TE and TM modes for this waveguide is given in table 7.3. Since the best rectangular waveguide result obtained is accurate to more

	TE k_c	TM k_c
1	1.84118378134066	2.40482555769570
2	1.84118378134066	3.83170597020752
3	3.05423692822714	3.83170597020752
4	3.05423692822714	5.13562230184026
5	3.83170597020751	5.13562230184026
6	4.20118894121053	5.52007811028631
7	4.20118894121053	6.38016189592398
8	5.31755312608399	6.38016189592398
9	5.31755312608399	7.01558666981560
10	5.33144277352504	7.01558666981560
11	5.33144277352504	7.58834243450380
12	6.41561637570009	7.58834243450380

Table 7.3: First 12 cutoff wave numbers k_c of a circular waveguide of radius 1 m.

than nine significant digits, great care has to be taken to obtain accurate analytical results. For this reason, the wave numbers are tabulated to double precision.

The RMS error over the first 12 modes is shown in Fig. 7.7. It is clear that the geometrical error made by the straight elements, dominate the results of all the basis functions, bar the CT/LN result.

The CT/LN result shows a similar error, and rate of convergence to the CT/LN result of the rectangular waveguide. All the other basis functions converge at the same rate as the CT/LN basis, while being less efficient, due to the DOFs wasted modelling the "wrong" geometry. From this one may

(a) RMS Error over 12 TE modes
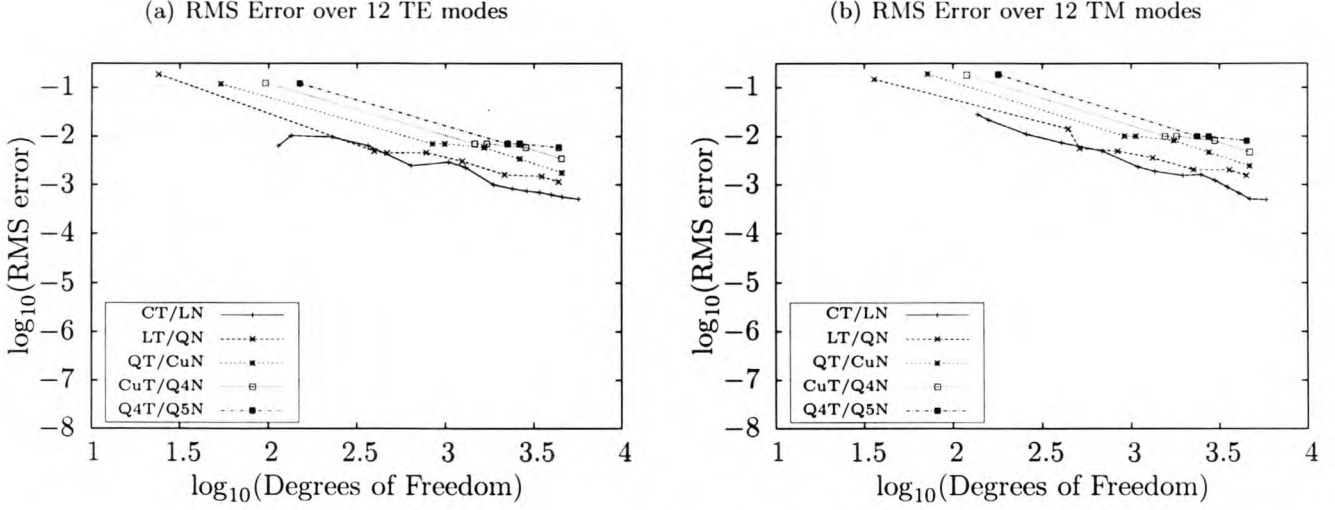
(b) RMS Error over 12 TM modes

Figure 7.7: Performance of Unmapped Elements: Circular Waveguide

conclude that the error made by the straight sided geometry, converges at a similar rate to the error made by the CT/LN basis.

7.3 Mapped Elements in Domains with Curved Boundaries

The performance of mapped (curved) elements are investigated in this section. In addition to the circular geometry considered in §7.2.3, mapped elements were also applied to a coaxial geometry, and an elliptic geometry, as respectively described in §7.1.5 and §7.1.4.

The coaxial geometry considered has a 1 m inner radius. The outer radius was chosen to give it a TEM mode, characteristic impedance of 50 Ω. The elliptical geometry considered, has a 1 m major axis, and an ellipticity of 0.5. Their respective modes are given in table 7.4. Only the TE modes of the elliptic waveguide are considered.

7.3.1 Mapped Mixed Order Elements

The performance of various coordinate mappings and bases are shown in figures 7.8, 7.9 and 7.10. The figures show, respectively, the circular, coaxial, and elliptic waveguide results.

The results of the QT/CuN and higher order bases are, in all cases, many orders of magnitude better than for the unmapped case. Note that the coarsest circular mesh did not have enough DOFs to produce 12 modes when used with the CT/LN elements.

59

|	Coaxial Waveguide		Elliptic Waveguide
	TE k_c	TM k_c	TE k_c
1	0.61863226004627	2.39625474992949	1.8510019462685945
2	0.61863226004627	2.47655373692904	2.1123640507905401
3	1.21239089155961	2.47655373692904	3.2226614791568795
4	1.21239089155961	2.70147634821676	3.2931582100347194
5	1.76718273849640	2.70147634821676	4.1904957369323785
6	1.76718273849640	3.03469737821871	4.4791693782254374
7	2.28529661776413	3.03469737821871	4.4947066374670666
8	2.28529661776413	3.43896312988662	5.5684326331812635
9	2.47655373692904	3.43896312988662	5.6816345961913068
10	2.57609903043474	3.88570073354709	5.684645915921319
11	2.57609903043474	3.88570073354709	5.9962093718266454
12	2.77837104064020	4.35575183555213	6.8588358186039224

Table 7.4: First 12 cutoff wave numbers k_c of a coaxial, and an elliptic waveguide. The coaxial waveguide has an inner radius of $a = 1$ m and a $50 = \Omega$ TEM characteristic impedance. The elliptic waveguide has a major axis $a = 1$ m, and an ellipticity of 0.5.

Figure 7.8: Performance of Mapped Elements: Circular Waveguide
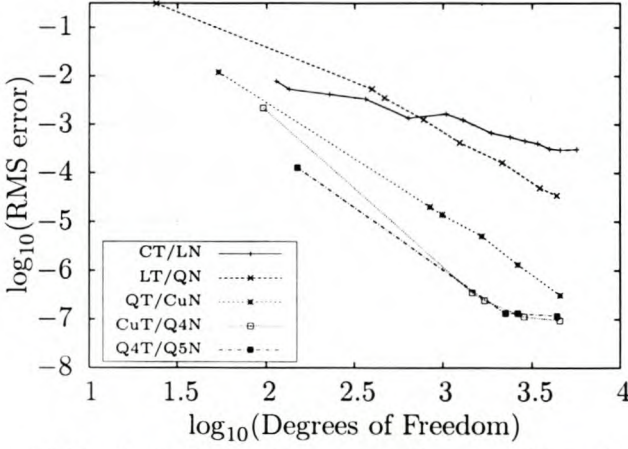
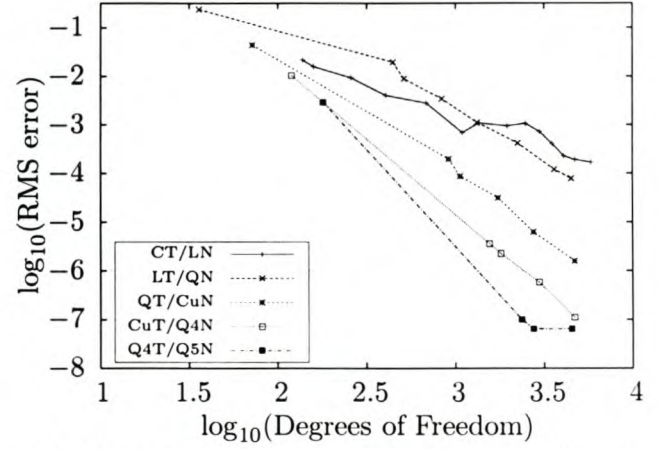(a) Quadratic Mapping, TE Modes
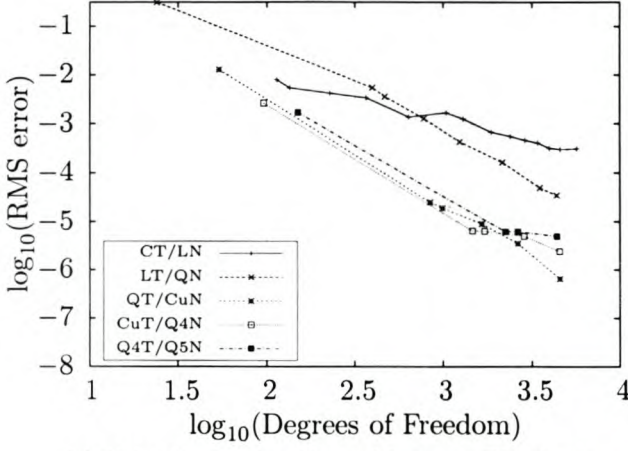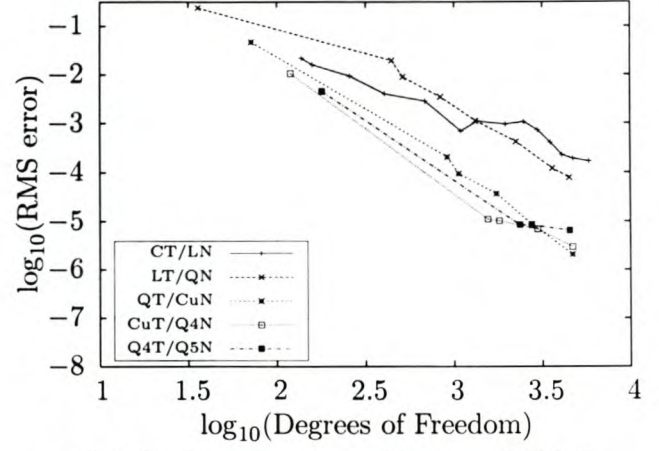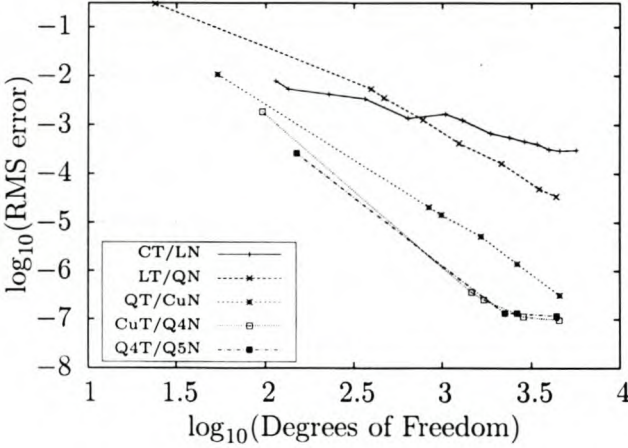
(b) Quadratic Mapping, TM Modes

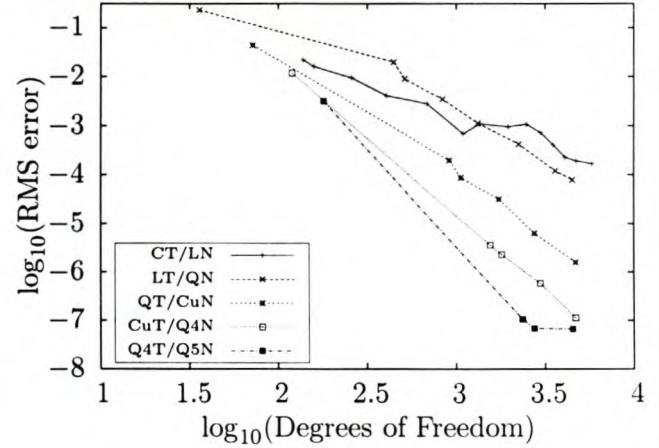(c) Cubic Parametric Curve Mapping, TE Modes

(d) Cubic Parametric Curve Mapping, TM Modes

(e) Quadratic Rational Parametric Mapping, TE modes

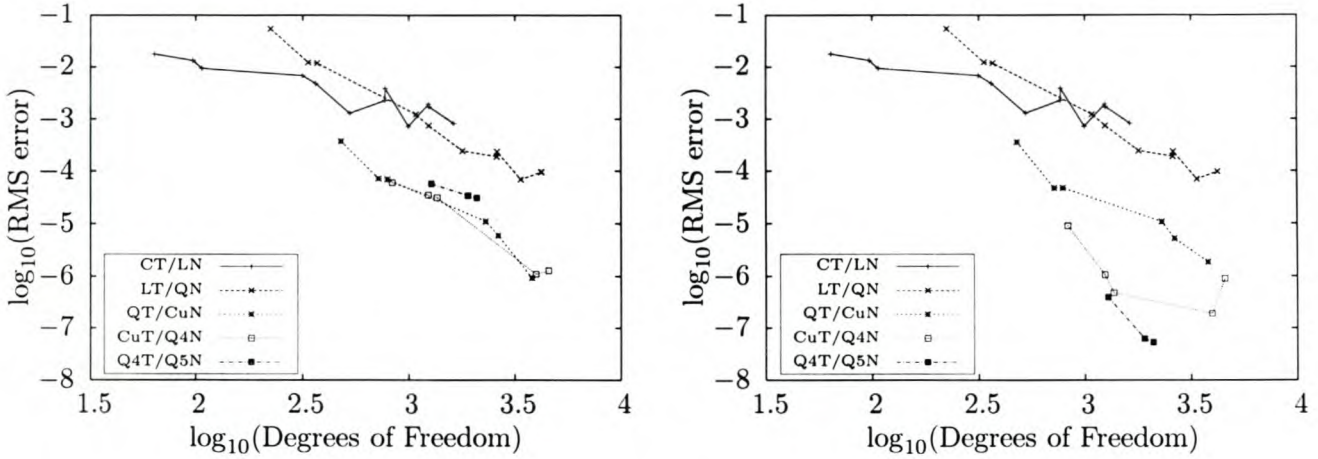(f) Quadratic Rational Parametric Mapping, TM modes

Figure 7.9: Performance of Mapped Elements: Elliptic Waveguide

(a) Quadratic Mapping, TE Modes   (b) Cubic Parametric Curve Mapping, TE Modes

An exception to the generally better performance of the mapped elements, is shown by the performance of the LT/QN basis functions on the two coarsest meshes. Table 7.5 shows the errors for the RMS error over 12 modes, and the individual errors for the first four modes of the circular waveguide. The RMS error is greater for the mapped elements when the two coarsest meshes are used. The individual errors of the lower order modes are, however, much smaller when the mapped elements are used.

Map	DOFs	$\log_{10}$ RMS error	Error percentage			
			Mode 1	Mode 2	Mode 3	Mode 4
Unmapped	24	-0.7247	5.8683	5.8683	-4.6273	-4.6273
Quadratic	24	-0.5040	-0.2419	-0.2419	-6.6576	-6.6576
Unmapped	396	-2.3061	0.5504	0.5506	0.5047	0.5069
Quadratic	396	-2.2640	-0.0031	-0.0029	-0.0352	-0.0336
Unmapped	780	-2.3340	0.4501	0.4503	0.4270	0.4281
Quadratic	780	-2.8934	-0.0013	-0.0010	-0.0076	-0.0071

Table 7.5: Circular waveguide LT/QN TE errors, mapped vs. unmapped
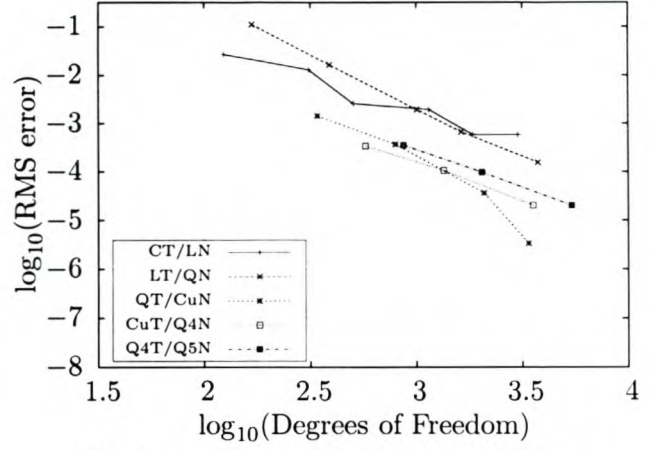
The quadratic mapping seems to be inadequate for bases of order higher than QT/CuN. The coaxial waveguide shows this especially clearly. The cubic parametric mapping performs almost identically to the exact, quadratic rational parametric mapping.

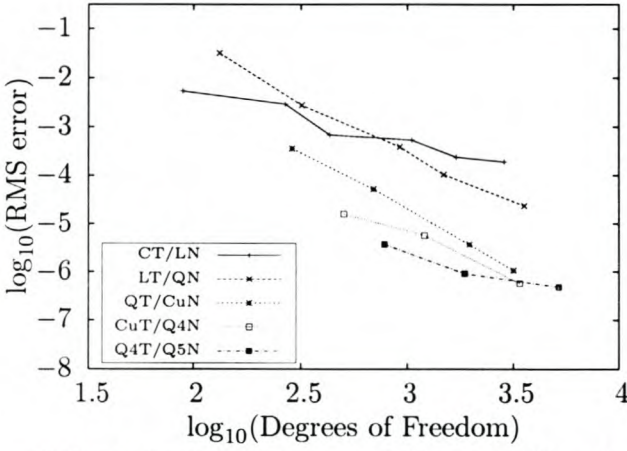Figure 7.10: Performance of Mapped Elements: Coaxial Waveguide
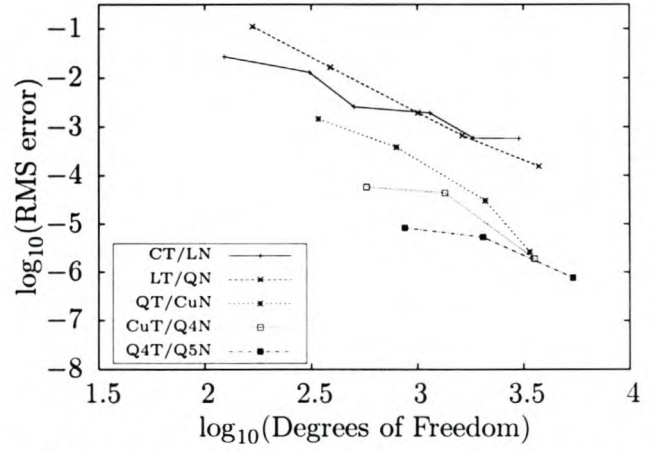
(a) Quadratic Mapping, TE Modes
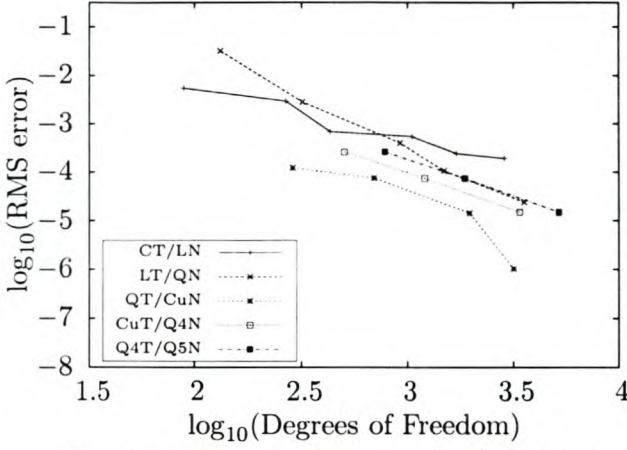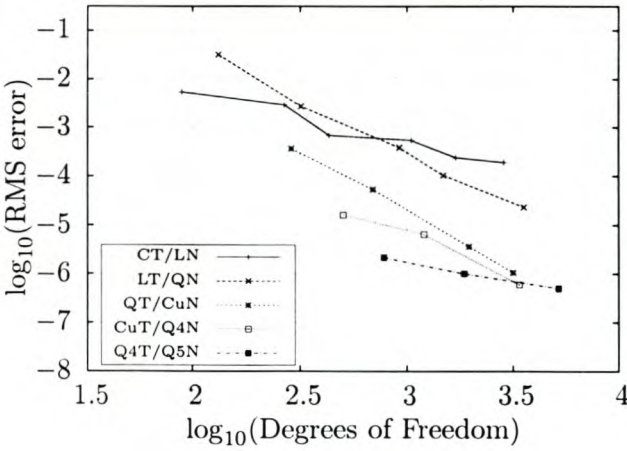
(b) Quadratic Mapping, TM Modes

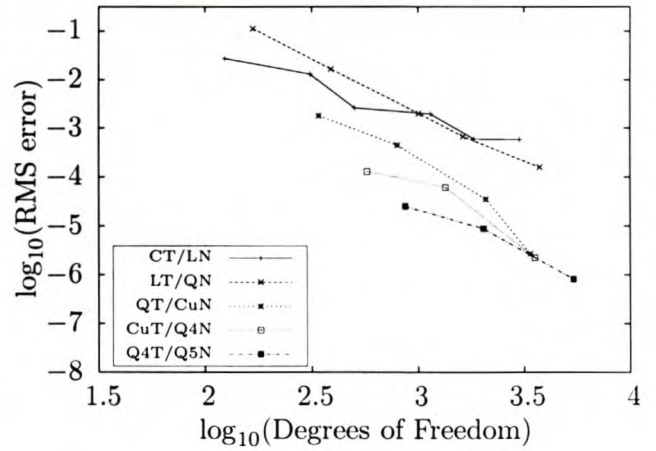(c) Cubic Parametric Curve Mapping, TE Modes

(d) Cubic Parametric Curve Mapping, TM Modes

(e) Quadratic Rational Parametric Mapping, TE modes

(f) Quadratic Rational Parametric Mapping, TM modes

63

Mapped bases of order QT/CuN and lower show, on curved geometries, a performance on par with that of unmapped bases on straight geometries. The best results the higher order mapped bases achieve on curved geometries, are similar to that of the QT/CuN base, and they do not show the expected order of asymptotic convergence.

The best results achieved for curved geometries, have an RMS error of about 10^{-7}. This is a significantly worse than the RMS error of about 10^{-9} achieved for the rectangular guide, and a similar number of DOFs. This seems to be the result of the mesher used, which exports mesh node positions with only five significant figures.

	Rectangular		Circular		Coaxial	
	TE	TM	TE	TM	TE	TM
CT/LN	0.93	0.83	0.85	1.21	0.81	0.68
LT/QN	1.89	2.27	1.61	1.55	2.38	1.70
QT/CuN	2.96	2.93	2.37	2.65	2.43	3.21
CuT/Q4N	3.91	4.40	2.54	3.57	1.34	2.53
Q4T/Q5N	4.63	4.20	2.10	3.41	1.03	0.75

Table 7.6: Convergence Rates of Various Bases

The convergence rates (ie. gradient of the error graph) of the various bases, are shown for several geometries in table 7.6. The triangle edge length h is inversely proportional to the square root of the number of triangles on a 2D domain. The convergence rate with respect to h is thus twice as fast as the convergence shown in table 7.6.

The rectangular results show close to the expected $O(h^{2p})$ convergence result. The mapped elements maintain the expected convergence rate for bases of order QT/CuN and lower.

7.3.2 Effects of Using Higher Order Integration

The quadrature scheme used to integrate the basis functions, are capable of exactly calculating polynomial integrands of a given order. As mentioned in §3.4, the basis functions of a mapped element are no longer polynomial. In light of this, it might be beneficial to use a higher order integration scheme than would be needed to integrate the unmapped basis functions exactly.

Since the Jacobian of a valid mapping is bounded from above, and below, the asymptotic behaviour of a given base is expected to be unchanged once mapped. Once might expect some improvement in the pre-asymptotic region, however.

Fig. 7.11 shows the performance of some lower order bases, with higher order integration. The notation LT/LN+2 refers to the fact that an integration order higher by two than required was used. The results with, and without, the higher order integration was almost identical. There does not seem to any advantage to using higher order integration than needed for the unmapped elements.
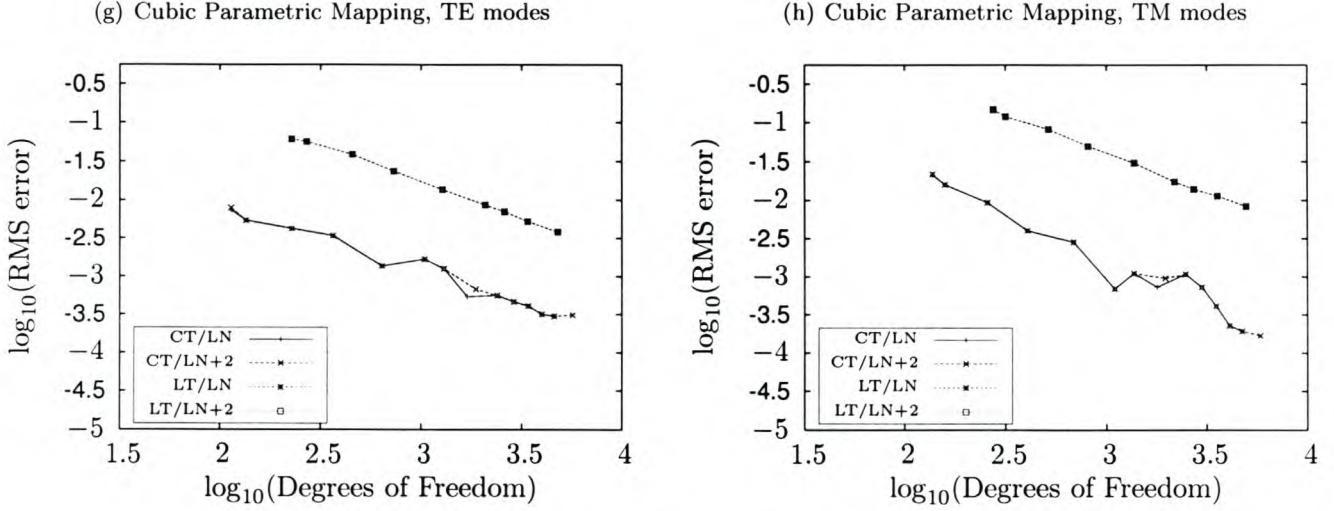
(g) Cubic Parametric Mapping, TE modes   (h) Cubic Parametric Mapping, TM modes

Figure 7.11: Performance of Mapped Elements with Higher Order Integration: Circular Waveguide

7.3.3 Conclusion

In this chapter, the performance of the higher order curvilinear elements developed in the previous chapters were evaluated. They were evaluated w.r.t. solution efficiency, on three curved, and one straight geometry, all of which have known analytical solutions.

It was shown that straight elements are woefully inadequate for higher order bases in curved geometries. It was shown that curvilinear elements can overcome the difficulty of modelling a curved geometry, and is able to match the performance of unmapped elements in domains with straight sides, provided the provided mesh is accurate enough.

It was seen that even very coarse meshes can provide accurate results, with higher-order, curved elements. In the case of the circular waveguide, the coarsest mesh used, consisted of only seven triangles.

It was established that a quadratic geometry mapping is adequate to maintain the performance of bases up to a curl order of 2 (QT/CuN). The requirements of the higher order bases could not be established, due to inaccuracies in the output of the mesher used.

Chapter 8

Conclusion

In the introduction, the need for higher order bases, and curvilinear elements was established. The aim of implementing both higher order bases, and curvilinear elements was set. Both goals were met.

The basic FEM formulation used was laid out. It was shown how one might apply basic vector elements to the functional formulation given by Jin. This provided a base for the rest of the work to build upon.

The theory of curvilinear, or general, coordinate systems were discussed, in light of a literature survey of the Electronic Engineering literature. A relative paucity of literature covering curved vector elements were found.

The reference triangle cell to be mapped onto curved geometries was presented. It was shown how covariant projection mapping could be used to construct curl-conforming, curved elements, using basis functions defined for vector simplexes.

The theory of polynomial functional spaces was discussed, in light of implementing basis functions of theoretically infinite order. This theory was implemented using a CAS, which resulted in high order bases being very easy to implement.

Bases up to full fifth order was implemented. These bases were first tested in a domain with straight sides, using plain simplexes with straight sides. The basis functions exhibited rates of convergence which were in agreement with the theoretical predictions.

Various mappings were applied to the previously developed bases. These mapped elements were tested with several curved geometries for which analytical solutions are known. They showed an improvement in performance of several orders of magnitude, as compared to unmapped elements in the same domains. Their ultimate performance was somewhat worse than that of the unmapped elements in straight domains, due to limitations of the mesher used.

Bibliography

[1] P. Silvester and R. L. Ferrari, *Finite elements for electrical engineers*. Cambridge University Press, 1996.

[2] J. Jin, *The Finite Element Method in Electromagnetics*. New York: John Wiley and Sons, 1993.

[3] T. Itoh, G. Pelosi, and P. P. Silvester, eds., *Finite Element Software for Microwage Engineering*. John Wiley & Sons, 1996.

[4] J. P. Webb, "Edge elements and what they can do for you," *IEEE Transactions on Magnetics*, vol. 29, pp. 1460–1465, March 1993.

[5] D. S. Burnett, *Finite Element Analysis from Concepts to Applications*. Addison-Wesley Publishing Company, 1998.

[6] J. S. Savage, "Higher-order vector finite elements for tetrahedral cells," *IEEE Transactions on Microwave Theory and Techniques*, vol. 44, pp. 874–879, June 1996.

[7] J. P. Webb and B. Forghani, "Hierarchal scalar and vector tetrahedra," vol. 29, pp. 1495–1498, March 1993.

[8] R. D. Graglia, D. R. Wilton, and A. F. Peterson, "Higher order interpolatory vector bases for computational electromagnetics," *IEEE Transactions on Antennas and Propagation*, vol. 45, pp. 329–342, March 1997.

[9] J. P. Webb, "Hierarchal vector basis functions of arbitrary order for triangular and tetrahedral finite elements," *IEEE Transactions on Antennas and Propagation*, vol. 47, pp. 1244–1253, August 1999.

[10] M. M. Botha, *Efficient finite element electromagnetic analysis of antennas and microwave devices: the FE-BI-FMM formulation and a posteriori error estimation for p adaptive analysis*. PhD thesis, Stellenbosch University, September 2002.

[11] F. J. C. Meyer and D. B. Davidson, "Adaptive-mesh refinement of finite-element solutions for two-dimensional electromagnetic problems," *IEEE Antennas and Propagation Magazine*, vol. 37, pp. 77–83, October 1996.

[12] D. Villeneuve and J. P. Webb, "Exact treatement of curved boundaries in large finite elements by re-parameterization," *IEEE Transactions on Magnetics*, vol. 36, pp. 1527–1530, July 2000.

[13] M. Zlámal, "The finite element method in domains with curved boundaries," *International Journal for Numerical Methods in Engineering*, vol. 5, pp. 367–373, 1973.

[14] E. Martini and S. Selleri, "Innovative class of curvilinear tetrahedral elements," *IEE Electronics Letters*, vol. 37, pp. 557–558, April 2001.

[15] G. Mur and A. T. de Hoop, "A finite-element method for computing three-dimensional electromagnetic fields in inhomogeneous media," *IEEE Transactions on Magnetics*, vol. MAG-21, pp. 2188–2191, November 1985.

[16] Z. J. Cendes, "Vector finite elements for electromagnetic field computation," *IEEE Transactions on Magnetics*, vol. 27, pp. 3958–3966, September 1991.

[17] J. F. Lee, D. K. Sun, and Z. J. Cendes, "Full-wave analysis of dielectric waveguides using tangential vector finite elements," *IEEE Transactions on Microwave Theory and Techniques*, vol. 390, pp. 1262–1271, August 1991.

[18] D. M. Pozar, *Microwave Engineering*. John Wiley & Sons, 2nd ed., 1998.

[19] N. Marcuvitz, *Waveguide Handbook*, vol. 21 of *IEE Electromagnetic Waves Series*. Peter Peregrinus. On behalf of The Institution of Electrical Engineers, 1986. Originally published in 1951.

[20] D. Hearn and M. P. Baker, *Computer Graphics*. Prentice-Hall International, 2nd ed., 1994.

[21] C. Ollivier-Gooch, *Generation and Refinement of Unstructured Mixed-Element Meshes in Parallel*. The University of British Columbia and The University of Chicago, `http://tetra.mech.ubc.ca/GRUMMP/`.

[22] D. B. Davidson, "Implementation issues for three-dimensional vector FEM programs," *IEEE Antennas and Propagation Magazine*, vol. 42, pp. 100–107, December 2000.

BIBLIOGRAPHY

[23] G. van Rossum *et al.*, *Python*. `http://www.python.org`.

[24] D. Ascher, P. F. Dubois, K. Hinsen, J. Hugunin, T. Oliphant, *et al.*, *Numerical Python*. `http://numpy.sourceforge.net/`.

[25] E. Anderson, Z. Bai, C. Bischof, S. Blackford, J. Demmel, J. Dongarra, J. Du Croz, A. Greenbaum, S. Hammarling, A. McKenney, and D. Sorensen, *LAPACK Users' Guide*. Philadelphia, PA, or `http://www.netlib.org/lapack/lug/lapack_lug.html`: Society for Industrial and Applied Mathematics, 3rd ed., 1999.

[26] R. C. Whaley, A. Petitet, *et al.*, *Automatically Tuned Linear Algebra Software*. `http://math-atlas.sourceforge.net/`.

[27] C. W. Crowley, P. P. Silvester, and H. Hurwitz Jr., "Covariant projection elements for 3D vector field problems," *IEEE Transactions on Magnetics*, vol. 24, pp. 397–400, January 1988.

[28] S. Caorsi, P. Fernandes, and M. Raffetto, "Do covariant projection elements really satisfy the inclusion condition?," *IEEE Transactions on Microwave Theory and Techniques*, vol. 45, pp. 1643–1644, September 1997.

[29] J. P. Webb and R. Miniowitz, "Analysis of 3-D microwave resonators using covariant-projection elements," *IEEE Transactions on Microwave Theory and Techniques*, vol. 39, pp. 1895–1899, November 1991.

[30] R. Miniowitz and J. P. Webb, "Covariant-projection quadrilateral elements for the analysis of waveguides with sharp edges," *IEEE Transactions on Microwave Theory and Techniques*, vol. 39, pp. 501–505, March 1991.

[31] B. R. Crain and A. F. Peterson, "Analysis of propagation on open microstrip lines using mixed-order covariant projection vector finite elements," *International Journal of Microwave and Millimeter-Wave Computer-Aided Engineering*, vol. 5, no. 2, pp. 59–67, 1994.

[32] A. Freni, M. C., and R. L. Ferrari, "Hybrid finite-element analysis of electromagnetic plance wave scattering from axially periodic cylindrical structures," *IEEE Transactions on Antennas and Propagation*, vol. 46, pp. 1859–1866, December 1998.

[33] A. Freni, C. Mias, and R. L. Ferrari, "Finite element analysis of electromagnetic wave scattering by a cylinder moving along its axis surrounded by a longitudinal corrugated structure," *IEEE Transactions on Magnetics*, vol. 32, pp. 874–877, May 1996.

BIBLIOGRAPHY

[34] J. S. Wang and N. Ida, "Curvilinear and higher order 'edge' finite elements in electromagnetic field computation," *IEEE Transactions on Magnetics*, vol. 29, pp. 1491–1494, March 1993.

[35] Y. Xiao and Y. Lu, "The hybrid perfectly matched layer and finite element solution for open region problems," *IEEE Transactions on Magnetics*, vol. 36, pp. 1635–1639, July 2000.

[36] J. Liu and J. M. Jin, "A special higher order finite-element method for scattering by deep cavities," *IEEE Transactions on Antennas and Propagation*, vol. 48, pp. 694–703, May 2000.

[37] A. F. Peterson and D. R. Wilton, *Curl-Conforming Mixed-Order Edge Elements for Discretizing the 2D and 3D Vector Helmholtz Equation*, ch. 5, pp. 101–125. In Itoh *et al.* [3], 1996.

[38] D. G. Zill and M. R. Cullen, *Advanced Engineering Mathematics*. PWS Publishing Company, 1992.

[39] A. S. Stratton, *Electromagnetic Theory*. McGraw-Hill Book Company, 1941.

[40] F. Ling, J. Liu, and J. M. Jin, "Efficient electromagnetic modeling of three-dimensional multilayer microstrip antennas and circuits," *IEEE Transactions on Microwave Theory and Techniques*, vol. 50, pp. 1628–1635, June 2002.

[41] G. Birkhoff, *The Numerical Solutions of Elliptic Equations*. Regional Conference Series in Applied Mathematics, Society for Industiral and Applied Mathematics, 1972.

[42] G. Mur, "The fallacy of edge elements," *IEEE Transactions on Magnetics*, vol. 34, pp. 3244–3247, September 1998.

[43] I. E. Lager and G. Mur, "Generalized Cartesian finite elements," *IEEE Transactions on Magnetics*, vol. 34, pp. 2220–2227, July 1998.

[44] W. F. Schelter *et al.*, *Maxima Manual.* `http://maxima.sourceforge.net/referencemanual/maxima_toc.html`.

[45] G. Mejak, "Curvilinear composite triangular element of class C^1," *Engineering Computations*, vol. 10, pp. 397–408, 1993.

[46] P. Bézier, *The Mathematical Basis of the Unisurf CAD System*. Butterworths, 1986.

[47] M. E. Mortenson, *Computer Graphics Handbook, Geometry and Mathematics*. Industrial Press, 1990.

BIBLIOGRAPHY

[48] G. Farin, "From conics to nurbs: A tutorial and survey," *IEEE Computer Graphics & Applications*, vol. 12, pp. 78–86, September 1992.

[49] M. Abramowitz and I. A. Stegun, eds., *Handbook of Mathematical Functions*. Dover Publications, 9th Dover ed., 1973.

[50] S.-j. Zhang and Y.-c. Shen, "Eigenmode sequence for an elliptical waveguide with arbitrary ellipticity," *IEEE Transactions on Magnetics*, vol. 43, pp. 227–230, January 1995.

[51] M. Schneider and J. Marquardt, "Fast computation of modified Mathieu functions applied to elliptical waveguide problems," *IEEE Transactions on Microwave Theory and Techniques*, vol. 47, pp. 513–515, April 1999.

[52] S. Wolfram, *The Mathematica Book*. Wolfram Media and Cambridge University Press, 4th ed., 1999.